We are IntechOpen, the world's leading publisher of Open Access books
Built by scientists, for scientists

6,900
Open access books available

186,000
International authors and editors

200M
Downloads

154
Countries delivered to

Our authors are among the

TOP 1%
most cited scientists

12.2%
Contributors from top 500 universities

CLARIVATE ANALYTICS
BOOK CITATION INDEX
INDEXED

WEB OF SCIENCE™

Selection of our books indexed in the Book Citation Index
in Web of Science™ Core Collection (BKCI)

Interested in publishing with us?
Contact book.department@intechopen.com

Mechanical Characterization of Laminated Rubber Bearings and Their Modeling Approach

A. R. Bhuiyan and Y.Okui

Additional information is available at the end of the chapter

1. Introduction

Base isolation, also known as seismic base isolation, is one of the most popular means of protecting a structure against earthquake forces. It is a collection of structural elements which should substantially decouple a superstructure from its substructure resting on a shaking ground thus protecting building and bridge structure's integrity. Base isolation is the most powerful tool of earthquake engineering pertaining to the passive structural vibration control technologies. It is meant to enable building and bridge structure to survive a potentially devastating seismic impact through a proper initial design or subsequent modifications. In some cases, application of base isolation can raise both a structure's seismic performance and its seismic sustainability considerably.

An isolation system is believed to be able to support a structure while providing additional horizontal flexibility and energy dissipation. Until the 80th decade of the last century many systems have been put forward involving features such as rollers or rockers bearings, sliding on sand or talc, or complaint first story column, but these have usually not employed in the practice of isolation of engineering structures [1, 2]. The study on the mechanical behavior of the isolation system dates back to 1886, when Professor Milne from Tokyo University, Japan attempted to observe isolation behavior of a structure supported by balls. He conducted an experiment by making an isolated building supported on balls "*cast-iron plates with saucer-like edges on heads of piles. Above the balls and attached to the buildings are cast-iron plates slightly concave but otherwise similar to those below*" [3]. However, another guy J.A. Calantarients in 1909, a medical doctor of the northern English City of Scarborough, was claimed to be the first man who conducted the experiment of isolation behavior of a structure supported by balls [3]. What both guys wanted to get information from their experiments is the global isolation behavior of the structure. The philosophy given by them regarding seismic isolation of a structure is stillin practice. Several mechanisms of

investigating the mechanical behavior of isolation systems are developed based on this philosophy which is readily used.

In practice of seismic base isolation of bridge structures, laminated rubber bearings have been popular since the last century. Among many types of laminated rubber bearings, natural rubber bearing (RB) which is formed by alternate layers of unfilled rubbers and steel shims has less flexibility and small damping. It has been used to sustain the thermal movement, the effect of pre-stressing, creep and shrinkage of the superstructures of the bridge or has been used for base isolation practices with additional damping devices [1, 2 and 4]. On the other hand, other two types of bearings possessing high damping were developed and have widely used in the seismic isolation practices [1, 3]. One is the lead rubber bearing (LRB), which additionally inserts lead plugs down the center of RB to enhance the hysteretic damping, and the other is high damping rubber bearing (HDRB), whose rubber material possesses high damping in order to supply more dissipating energy.

Following the same principle as Professor Milne used in his experiments, several authors conducted experimental studies on different bridge structures mounted on laminated rubber bearings. Kelly et al. [5] studied quarter-scale models of straight and skewed bridge decks mounted on plain and lead-filled elastomeric bearings subjected to earthquake ground motion using the shaking table. The deck response was compared to determine the effectiveness of mechanical energy dissipaters in base isolation systems and the mode of failure of base-isolated bridges. Igarashi and Iemura [6] evaluated the effects of implementing the lead-rubber bearing as seismic isolator on a highway bridge structure under seismic loads using the substructure hybrid loading (pseudo-dynamic) test method. The seismic response of the isolated bridge structure was successfully obtained. The effectiveness of isolation is examined based on acceleration and displacement amplifications using earthquake response results. All of their studies were related to observation of the isolation effects on the bridge structures. Very few works were undertaken in the past regarding the mechanical behavior of isolation bearings.

Mori et al. [7, 8] studied the behavior of laminated bearings with and without lead plug under shear and axial loads. They evaluated hysteretic parameters of the bearings: horizontal stiffness; vertical stiffness; and equivalent damping ratio. The similar study was conducted by Burstscher et al. [9]; Fujita et al. [10]; Mazda et al. [11] and Ohtori et al. [12] on lead, natural and high damping rubber bearings. They concluded from the experimental results that the hysteretic parameters have low loading rate-dependence. Furthermore, Robinson[13], a pioneer of developing and introducing the lead rubber bearing (LRB) as an excellent isolation system to be used in seismic design of civil engineering structures, conducted an elaborate experimental tests on LRB in order to describe the hysteretic behavior. From the experiments he concluded that the hysteretic behavior of the LRB can be expressed well by using a bilinear relationship of the force-displacements. In addition, he conducted some tests regarding fatigue and temperature performance of the LRB.

Several authors conducted different loading experiments on laminated rubber bearings (RB, LRB, and HDRB) in order to acquire deep understanding of the mechanical properties. In this case the works of Abe et al. [14]; Aiken et al. [15]; Kikuchi and Aiken [16]; Sano and D Pasquale [17] can be noted. They have applied uni-directional and bi-directional horizontal shear deformations with constant vertical compressive stress. Several types of laminated rubber bearings were used in their experimental scheme. In their investigations they identified some aspects of the bearings such as hardening features and dependence of the restoring forces on the maximum displacement amplitude experienced in the past. Moreover, some of them also identified coupling effects on the restoring forces of the bearings due to deformation in the two horizontal directions. Motivated by the experimental results of the bearings different forms of analytical models of the bearings were proposed by them. However, their studies were mostly related to illustrating the strain-rate independent mechanical behavior of the bearings.

Very few works are reported in literature regarding the strain-rate dependent behavior of the bearings. In this regard, the works of Dall'Asta and Ragni [18]; Hwang et al. [19] and Tsai et al. [20] can be reported. They studied the mechanical behavior of high damping rubber dissipating devices by conducting different experiments such as sinusoidal loading tests at different frequencies, simple cyclic shear tests at different strain-rates along with relaxation tests. From the experiments they have identified the strain-rate dependence of the restoring forces and subsequently developed rate-dependent analytical models of the bearings. Strain-rate dependent Mullin's softening was also identified in the experiments [18]. However, separation of the rate-dependent behavior from other mechanical behavior of the bearings was not elaborately addressed in their studies.

A number of experimental and numerical works on different rubber materials (HDR: high damping rubber and NR: natural rubber) have been performed in the past [21-27]. These works show that the mechanical properties of rubber materials (especially HDR) are dominated by the nonlinear rate-dependence including other inelastic behavior. Moreover, the different viscosity behavior in loading and unloading has been identified [21, 23, 28 and 29].

It is well known that since seismic response of base isolated structures greatly depends on mechanical properties of the bearings, deep understanding of the characteristics of the bearings under the desired conditions is very essential for rational and economic design of the seismic isolation system. The general mechanical behavior of laminated rubber bearings mainly concerns with nonlinear rate-dependent hysteretic property [18, 19] in addition to other inelastic behavior like Mullin's softening effect [30] and relaxation behavior [31]. All these characteristic behaviors generally originate from the molecular structures of the strength elements of rubber materials used in manufacturing of the bearings. Within this context, the chapter is devoted to discuss an experimental scheme used to characterize mechanical behavior and subsequently develop a mathematical model representing the characteristic behavior of the bearings.

2. Experimental observation

The objective of the work is to make qualitative and quantitative studies of strain-rate dependency of the bearings subjected to horizontal shear deformation with a constant vertical compressive load. To this end, an experimental scheme comprised of multi-step relaxation tests, cyclic shear tests, and simple relaxation tests was conducted: the mutli-step relaxation tests were carried out to investigate the strain-rate independent behavior along with viscosity behavior in loading and unloading; the cyclic shear tests, to observe the strain-rate dependency; and the simple relaxation tests, to describe the viscosity behavior of the bearings. To separate the Mullins' effect from other inelastic effects, a preloading sequence was applied on each specimen prior to the actual test. Details of the experiments and the inferences observed therein are described in the following subsections.

2.1. Specimens

The bearings manufactured and used in this study were divided into seven different types of specimens depending on their chemical compositions and damping properties: three types of high damping rubber bearings (HDR1, HDR2, and HDR3); two types of lead rubber bearings (LRB1, LRB2); and two types of natural rubber bearings (RB1, RB2). All the specimens had a square cross-sectional shape with external in-plane dimensions equal to 250 mm x 250 mm. The reinforcing steel plates had similarly a square planar geometry with external dimensions of 240 mm x 240 mm and thickness of 2.3 mm each. The geometry and material properties of these specimens are given in Table 1 and illustrated also in Figure 2. The dimensions of the test specimens were selected following the ISO standard [32]. Due to the space limitation the experimental results of three specimens, one HDRB (HDRB2), one RB (RB2) and one LRB (LRB2) are presented in the subsequent sections. However, the interested readers are requested to refer to the earlier efforts of the author [33-35] for better understanding to the rate-dependent mechanical behavior of the bearings. Figure 3 present typical actual bearing specimens used in the experiment in deformed and unreformed conditions.

2.2. Experimental set-up and loading conditions

A schematic detail of the experimental set-up is presented in Figure 1. The specimens were tested in a computer-controlled servo-hydraulic testing machine at room temperature (23 ^{0}C). Displacement controlled tests, under shear deformation with an average constant vertical compressive stress of 6 MPa, were carried out. This mode of deformation is regarded as the most relevant one for application in seismic isolation [2]. The displacement was applied along the top edge of the specimen and the force response was measured by two load cells. All data were recorded using a personal computer. Throughout this paper, to express the experimental results, the average shear stress and shear strain are calculated using the following two equations

$$\gamma = \frac{u}{h}, \tag{1}$$

$$\tau = \frac{F_h}{A}, \tag{2}$$

where u and F_h denote the relative horizontal displacement and applied force, respectively; h stands for the total thickness of rubber layers and A is the area of the cross section.

Specifications	High damping rubber bearing			Natural rubber bearing		Lead rubber bearing	
	HDR1	**HDR2**	HDR3	RB1	**RB2**	LRB1	**LRB2**
Cross-section (mm)	240X240			240X240		240X240	
Number of rubber layers	6			6		6	
Thickness of one rubber layer (mm)	5			5		5	
Thickness of one steel layer (mm)	2.3			2.3		2.3	
Diameter of lead plug (mm)	-			-		34.5	
No of lead plugs	-			-		4	
Nominal shear modulus (MPa)	1.2			1.2		1.2	

Table 1. Geometry and material properties of the bearings

2.2.1. Softening behavior

Virgin rubber typically exhibits a softening phenomenon, known as Mullins' effect in its first loading cycle. Due to presence of this typical behavior, the first cycle of a stress-strain curve differs significantly from the shape of the subsequent cycles [30]. In order to remove the Mullins softening behavior from other inelastic phenomena, all specimens were preloaded before the actual tests. The preloading was done by treating 11 cycles of sinusoidal loading at 1.75 strain and 0.05 Hz until a stable state of the stress-strain response is achieved, i.e., that no further softening occurs. The strain histories as applied in preloading sequence are shown in Figure 4.

Figures 5 (a), (b), and (c) present the typical shear stress-strain responses obtained from pre-loading tests on HDR2, RB2 and LRB2 specimens. The same loading sequence was applied on two types of specimens: virgin specimens and preloading specimens. The virgin specimen was loaded first with the prescribed loading sequence and then the same specimen (known as the preloading specimen) was again loaded with same loading sequence. The time interval between these two loading sequences was 30 min. The softening behavior in the first loading cycle is evident from Figure 5 in each specimen (virgin and preloading) indicating that the Mullins softening effect is not only present in the virgin specimen but also in any preloaded specimen [18]. This implies that Mullins effect can be

recovered in quite a very short period. This is certainly due to the 'healing effect' [36, 37]. As can be seen from Figures 5 (a) to (c), the softening behavior is more appreciably well-defined in HDR2 than LRB2 and RB2. All the specimens have shown a repeatable stress-stretch response after passing through 4-5 loading cycles indicating that the Mullin's softening effect of the bearings is removed from the other effects.

2.2.2. Strain-rate dependent behavior

With a view to understanding the mechanical behavior of the bearings regarding the strain rate-dependence, cyclic shear tests (CS tests) at different strain rates were carried out. In the test series, a number of constant strain-rate cases within a range of 0.05/s to 5.5/s were considered as shown in Figure 6. Figures 7 (a), (b), and (c) show the strain-rate dependent shear stress responses of HDR2, RB2, and LRB2 bearings, respectively. For comparison, the equivalent stress responses of the bearings are also represented in each Figure. The equivalent stress responses of the bearings can be identified from MSR test results (Section 2.2.4).
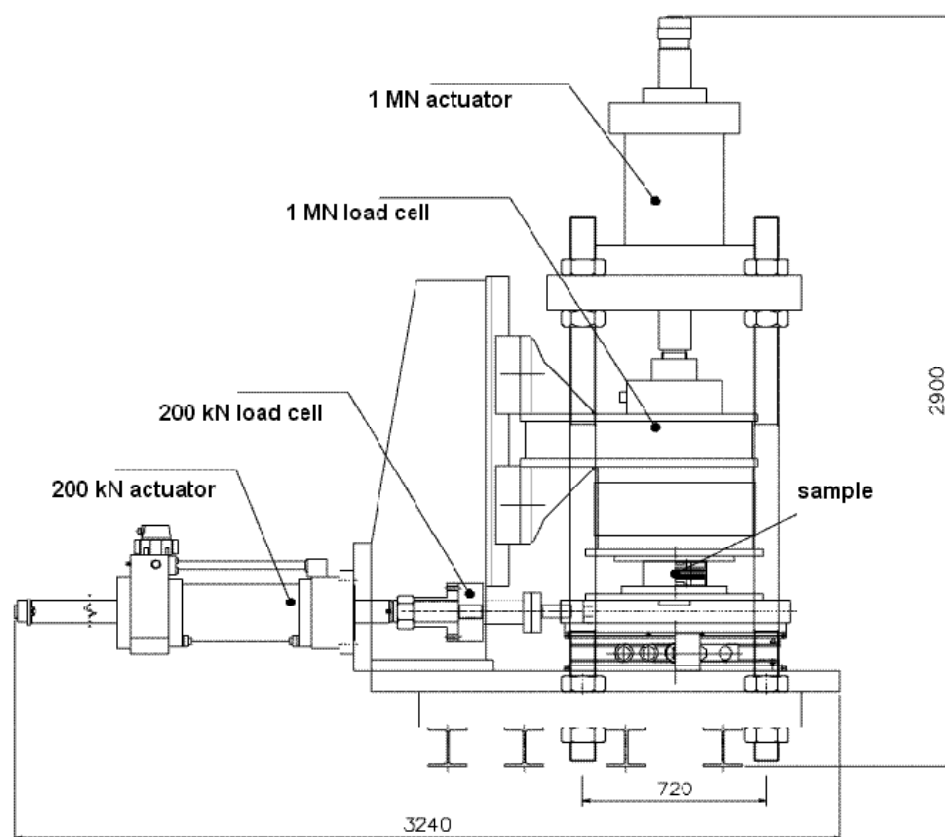

Figure 1. Schematic details of the experimental set-up. All dimensions are in mm

In general, the stress responses in the loading path contain three-characteristic features like a high initial stiffness feature at low strain levels followed by a traceable large flexibility at moderate strain levels as well as a large strain-hardening feature at the end. The untangling and/or the separation of weak bonds between filler particles and long chains are associated

with reduced effect of the high initial stiffness [38]. This typical phenomenon is regarded the 'Payne effect' [25]. The final increase of the stiffness is attributed to the limited extensibility of the polymer chains and may be endowed to the 'strain hardening' feature [38]. When compared among the three bearings, the high initial stiffness at a low strain level and the high strain hardening at a high strain level are mostly prominent in HDR2 at a higher strain rates. However, a weaker strain-hardening feature in LRB2 than the other specimen (RB2) at higher strain levels is also noticeable. A comparison of hysteresis loops observed at different strain rates shows that the size of the hysteresis loops increases with increase of strain rates
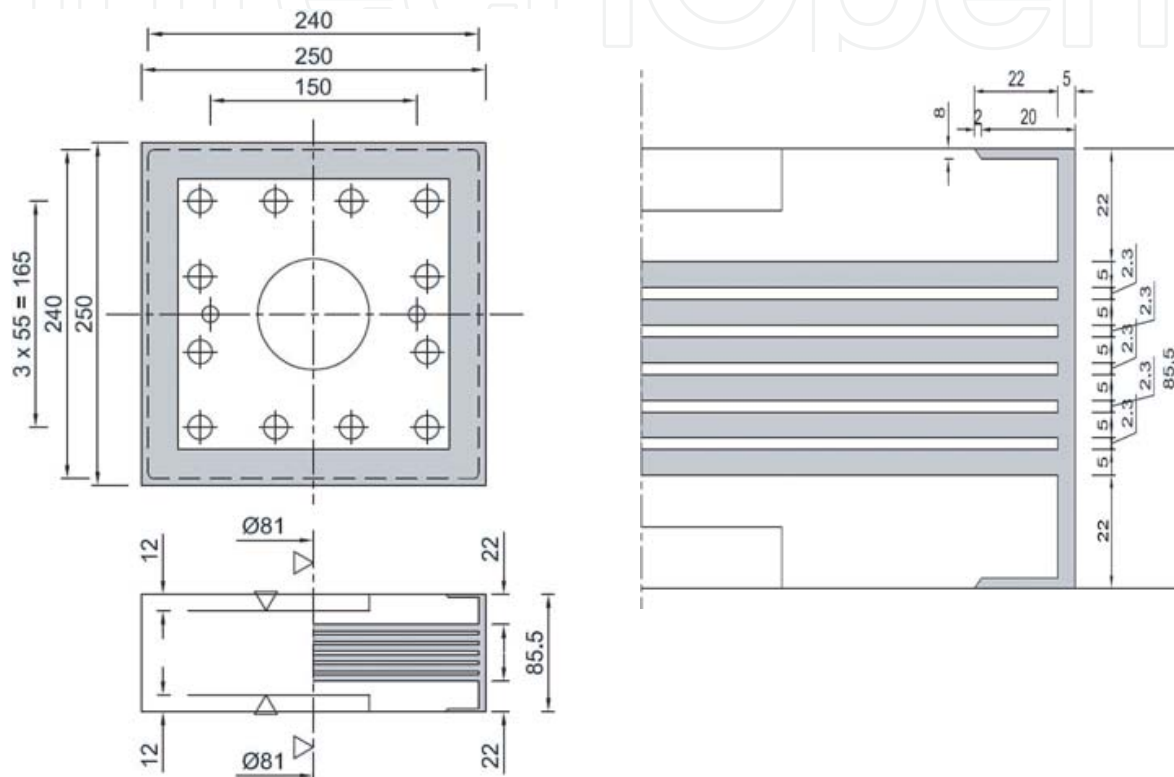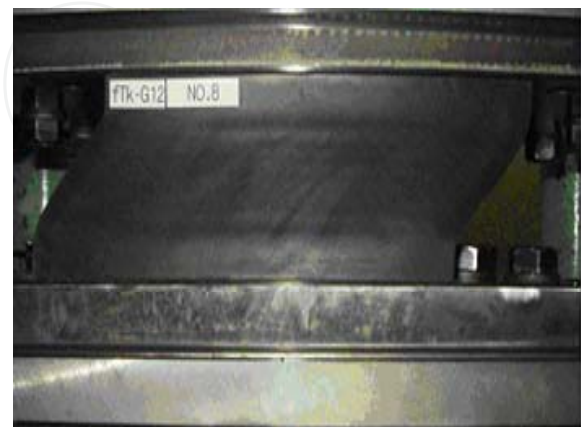

Figure 2. Dimension of a specimens [mm] (a) plan view (b) sectional view
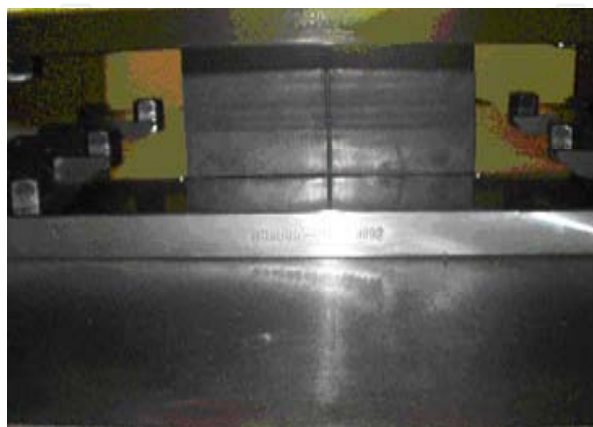
(a)   (b)

Figure 3. Typical bearing specimens used in the experiment in (a) un-deformed and (b) deformed condition

as shown in Figures 7 (a) to (c). While comparing among all the bearings, HDR2 demonstrates a bigger hysteresis loop compared with the other bearings (RB2 and LRB2). This typical behavior can be attributed that the HDR2 inherits relatively high viscosity property than in other bearings. The addition of special chemical compounds in manufacturing process enhances the damping property of the HDRB.
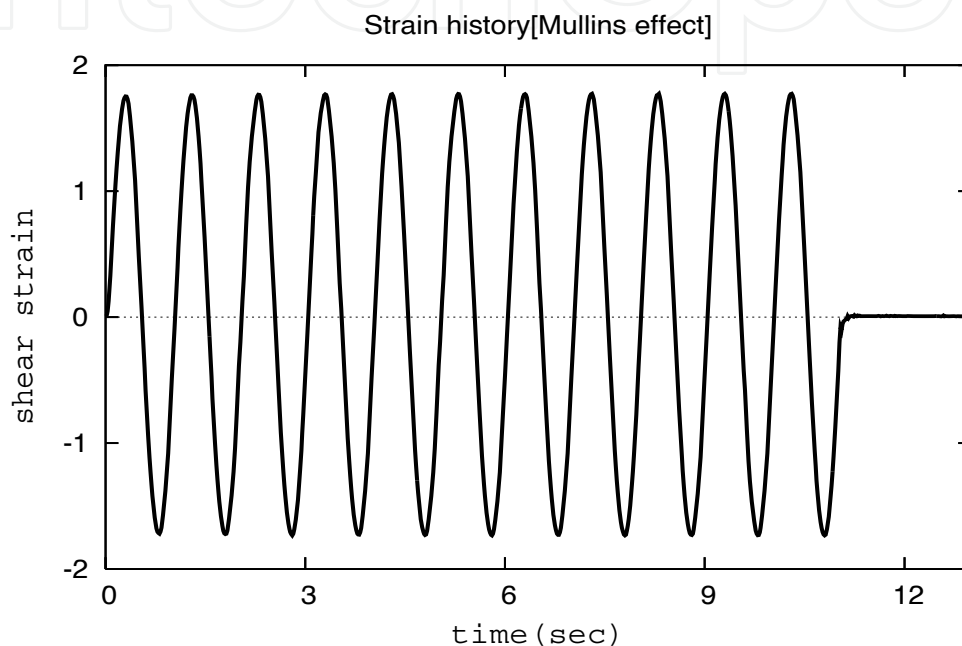

Figure 4. Applied strain histories in preloading test

Another comparison of the shear stress responses at different strain rates of the bearings shown in Figures 6(a) to (c) indicates that the strong strain-rate dependence exists in loading, whereas much weaker strain-rate dependence is observed in unloading. The different viscosity property in loading and unloading is attributed to this typical experimental observation. The basic strength elements of rubber are very long chain molecules, which are cross-linked with each other at some points to form a network [39]. Two types of linkages are occurred in rubber: physical linkages and chemical linkages. Due to the inherent properties of building up the physical and chemical linkages of rubber, the physical linkages are much weaker in stability and strength compared with the chemical linkages [40, 41]. The physical linkages have small energy capacity, which are easily broken; however, the chemical linkages have higher energy capacity, which require external energy to be broken. In loading at a particular strain rate, some of the physical and chemical linkages are broken, however, in unloading at the same strain rate; the breaking up the physical linkages is more prominent than the chemical linkages. These phenomena may be attributed to different viscosity behavior in loading and unloading of the bearings.

A further comparison among the loading-path responses at different strain-rates shows that the stresses increase due to viscosity with the increase of strain-rates. At higher strain rates, however, a diminishing trend in increase of stress responses is observed indicating an approach to the instantaneous state.
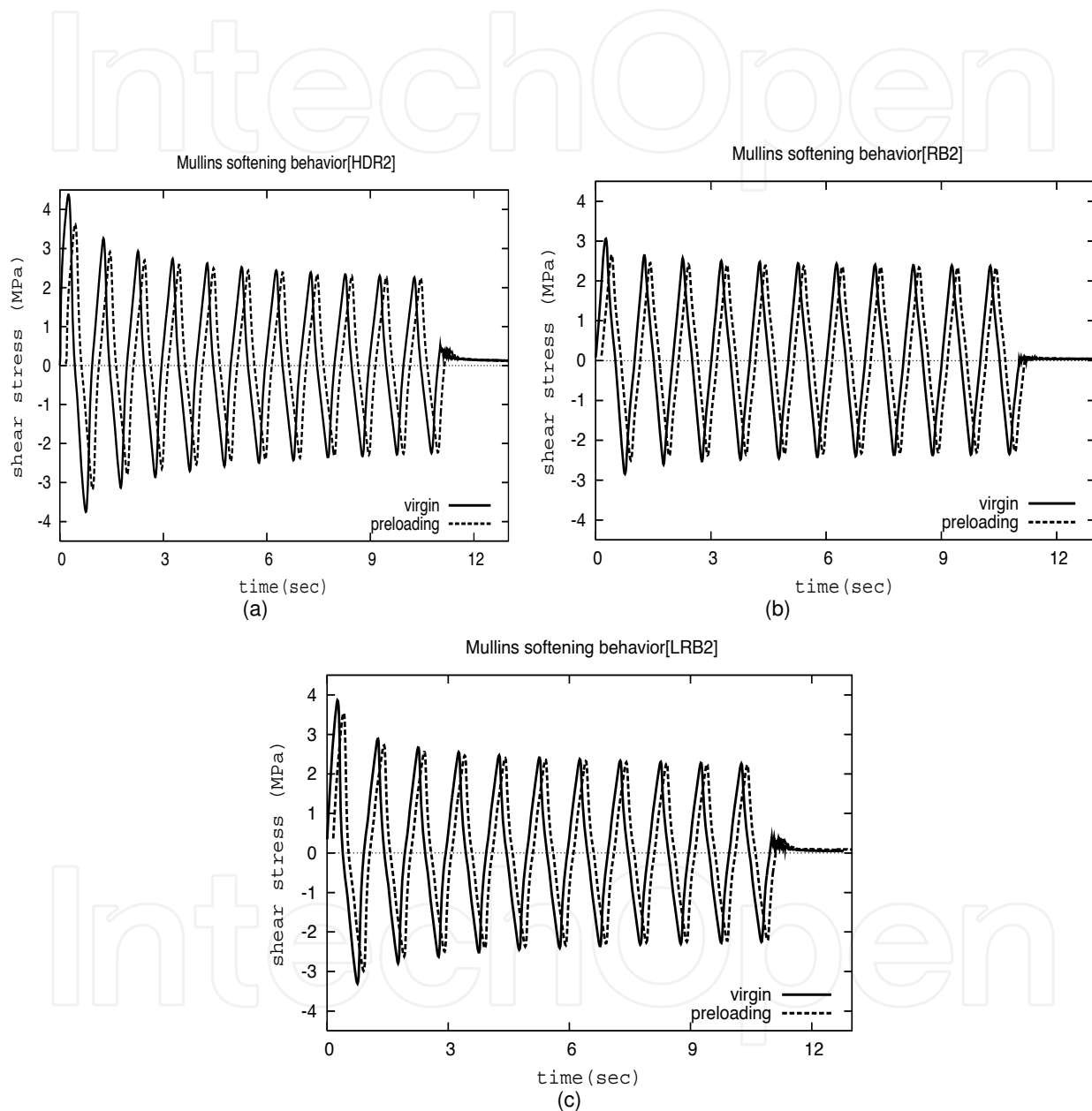

Figure 5. 11-cycle preloading test on the bearings to remove Mullins effect; (a) HDR2, (b) RB2, (c) LRB2; the legend indicates that the solid line in each Figure shows the shear stress histories obtained from the virgin specimens and the dotted line does for the preloading specimens. For clear illustration the shear stress-strain responses are separated by 0.15 sec from each other
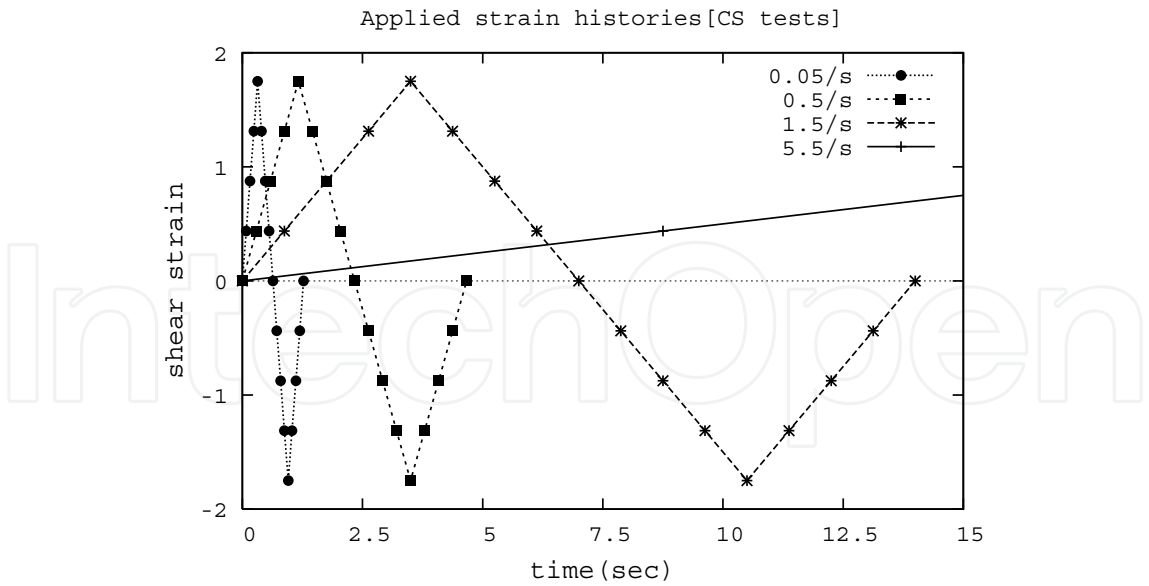
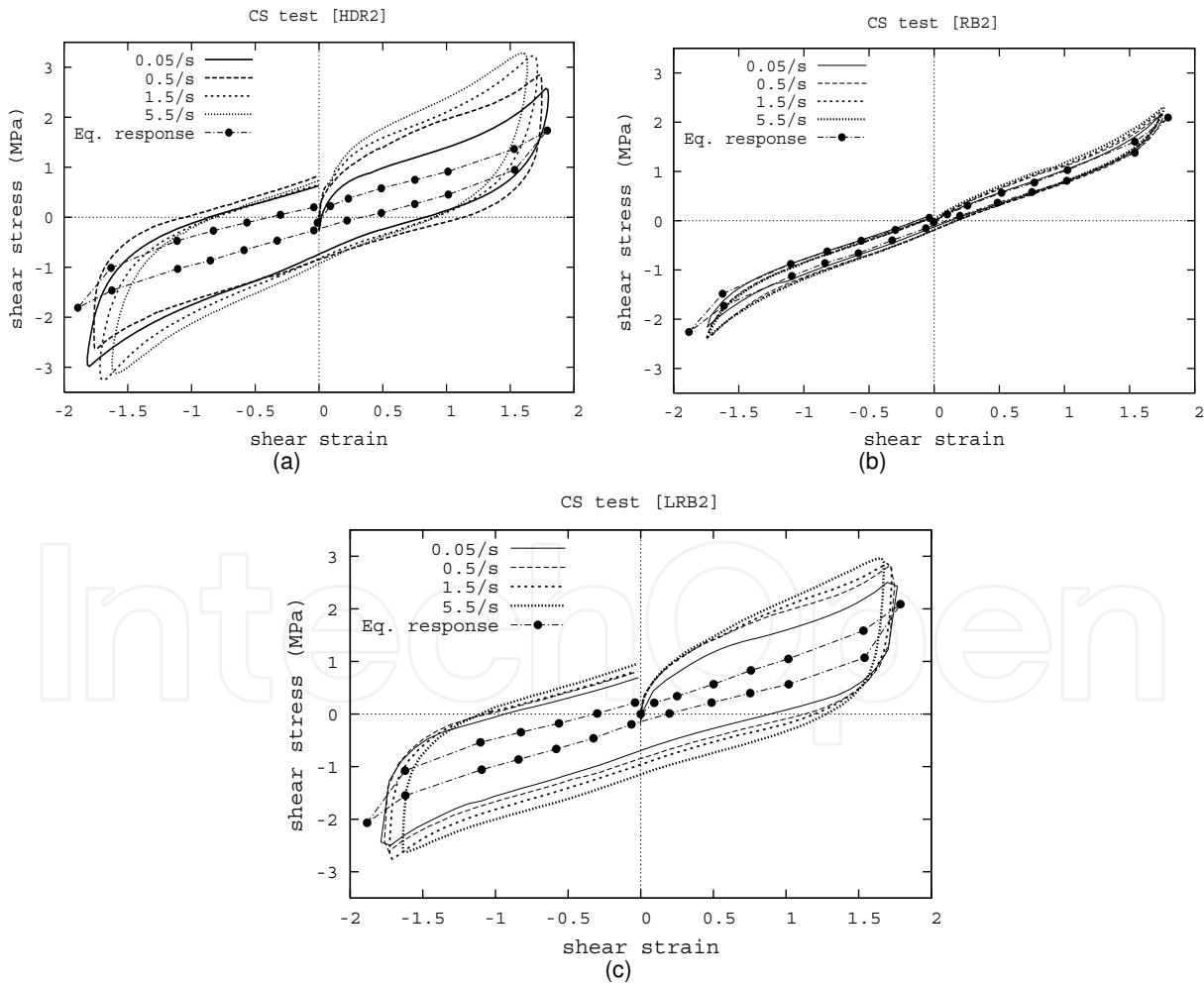**Figure 6.** Applied strain histories in CS tests.

Figure 7. Shear stress-strain relationships obtained from CS tests at different strain rates of the bearings; (a) HDR2, (b) RB2, (c)LRB2; equilibrium response as obtained from MSR tests is also presented for clear comparison.

2.2.3. Viscosity behavior

The cyclic shear tests presented in Section 2.2.2 revealed the existence of viscosity in all specimens. In this regard, simple relaxation (SR) tests were carried out to study the viscosity behavior of the bearings. To this end, a series of SR tests at different strain levels were carried out. Figure 8 shows the strain histories of SR loading tests at three different strain levels of γ = 100, 150, and 175% with a strain rate of 5.5/s in loading and unloading. The relaxation period in loading and unloading was taken 30 min.

The shear stress histories of the bearings as obtained in SR tests are presented in Figures 9 (a) to (c). The stress relaxation histories in each specimen illustrate the time dependent viscosity behavior of the bearings. For all specimens, a rapid stress relaxation was displayed in the first few minutes; after while it approached asymptotically towards a converged state of responses. The stress relaxation was observed in each specimen. The amount of stress relaxation in loading and unloading of HDR2 was found to be much higher than those obtained in other bearings (RB2 and LRB2). As can be seen from Figures 9 (a) to (c), HDR2 shows comparatively high stress relaxation than the other bearings. On the other hand, RB2 shows much lower stress relaxation than that of other bearings. These observations confirm the findings of the cyclic shear loading tests and interpretations as mentioned in the preceding section (Figures 7 (a) to (c)). The stress response obtained at the end of the relaxation can be regarded as the equilibrium stress response in asymptotic sense [25, 42]. The deformation mechanisms associated with relaxation are related to the long chain molecular structure of the rubber. In the relaxation test, the initial sudden strain occurs more rapidly than the accumulation capacity of molecular structure of rubber. However, with the passage of time the molecules again rotate and unwind so that less stress is needed to maintain the same strain level.
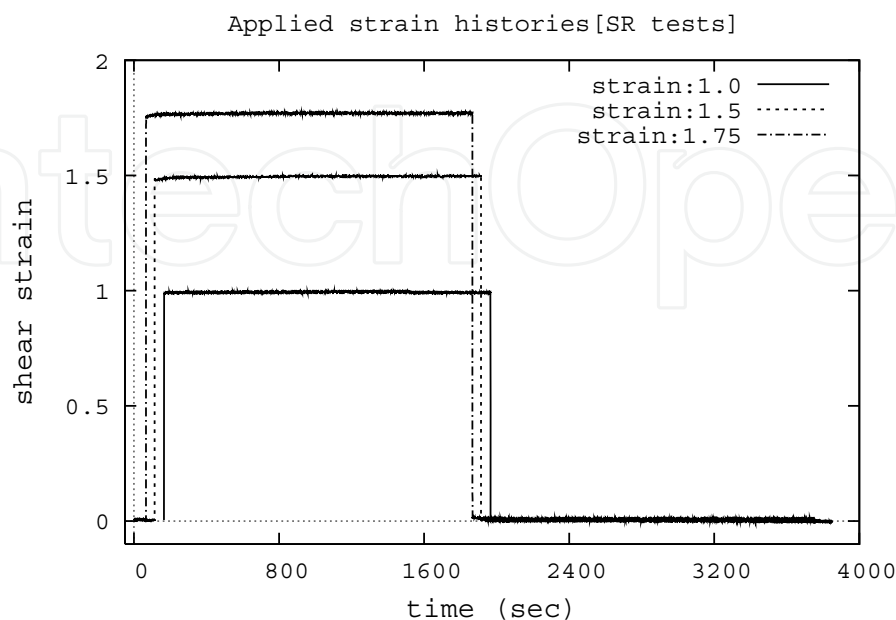

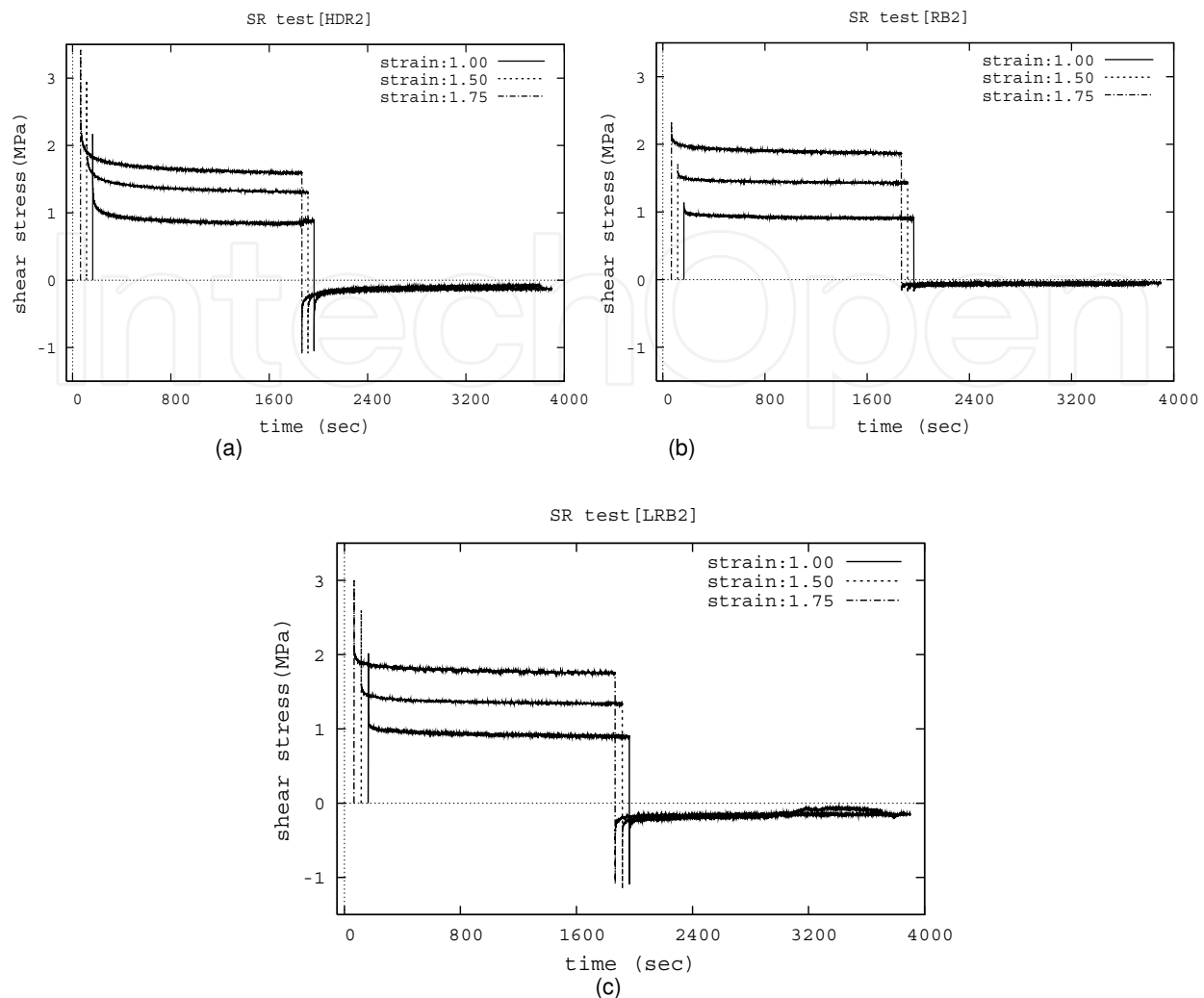**Figure 8.** Applied strain histories in SR test.

Figure 9. Shear stress histories obtained from SR tests of the bearings at different strain levels (a) HDR2, (b) RB2, (c) LRB2. For clear illustration, the stress histories have been separated by 50 sec to each other.

2.2.4. Static equilibrium hysteresis

The cyclic shear test results presented in Section 2.2.2 illustrated the strain-rate dependent property. The subsequent simple relaxation tests (Section 2.2.3) further explained the property. The tests carried out at different strain levels showed reduction in stress response during the hold time and approached the asymptotically converged states of responses (i.e equilibrium response). In this context, multi-step relaxation (MSR) tests were carried out to observe the relaxation behavior in loading and unloading paths and thereby to obtain the equilibrium hysteresis (e.g. strain-rate independent response) by removing the time-dependent effects.

The shear strain history applied in MSR test at 1.75 maximum strain level is presented in Figure 10, where a number of relaxation periods of 20 min during which the applied strain is held constant are inserted in loading and unloading at a constant strain rate of 5.5/s. Figures 11 to 13 illustrate the shear stress histories and corresponding equilibrium responses obtained in MSR tests of three bearings (HDR2, RB2, and LRB2). It is observed that at the end of each relaxation

interval in loading and unloading paths, the stress history converges to an almost constant state in all specimens (Figures 11 to 13). The convergence of the stress responses is identified in an asymptotic sense [25]. The shear stress-strain relationships in the equilibrium state can be obtained by connecting all the asymptotically converged stress values at each strain level as shown in Figures11 (b), 12(b) and 13(b). The difference of the stress values between loading and unloading at a particular shear strain level corresponds to the equilibrium hysteresis, which can be easily visualized in Figures 11 (b), 12(b) and 13(b). This behavior may be attributed due to an irreversible slip process between fillers in the rubber microstructures [30, 43], which is the resulting phenomenon of breaking of rubber-filler bonds [36,37]. Using the stress history data of Figures11 (a), 12(a) and 13(a), the overstress can be estimated by subtracting the equilibrium stress response from the current stress response at a particular strain level.

While comparing the overstress for each specimen as shown in Figures 11 (a), 12(a) and 13(a), the overstress in loading period is seen higher than in unloading at a given strain level. The maximum overstress was observed in HDR2 while in RB2 it was the minimum one. This typical behavior of the bearings is seen comparable with CS test results (Figures 7 (a) to (c)).
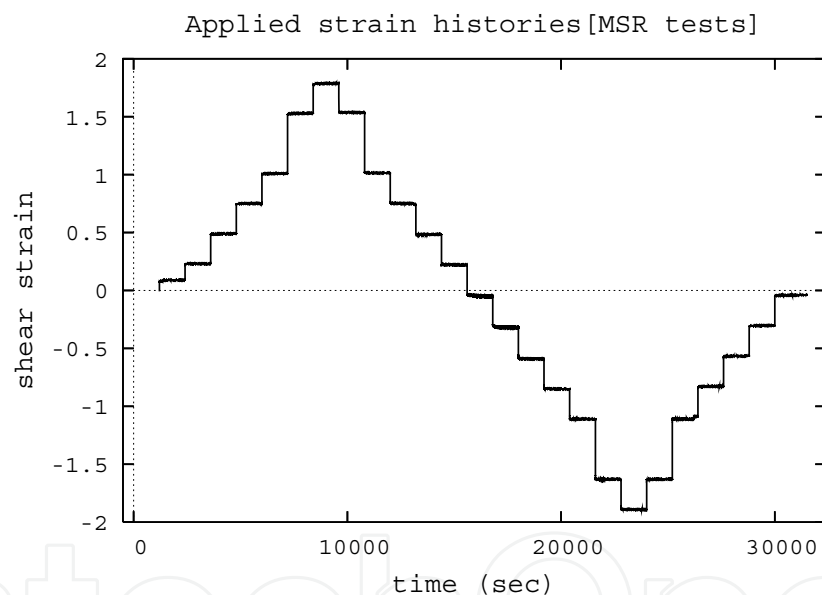

Figure 10. Applied strain histories in MSR test at 1.75 maximum strain level; a shear strain rate of 5.5/s was maintained at each strain step.

Furthermore, with a view to characterizing the strain hardening features along with dependence of the equilibrium hysteresis on loading history of the bearings, another set of multi-step relaxation tests were carried out at different maximum strain level of 2.5. Figures 14(a) and (b) present the results obtained in testing HDR2 due to the strain history of MSR test with maximum strain level of 2.5. Similar to the experiment carried out at the maximum strain level of 1.75, the equilibrium hysteresis effect is also observed in the MSR test; however, the magnitudes were found to increase with increasing strain level with increased supply of energy. Other sets of experiments similar to those in HDR2 were also carried out on other bearings. Figures 15 and 16 present the results on RB2 and LRB2. Although in

Figures 15 and 16 a trend similar to HDR2 in the appearance of equilibrium hysteresis was noticed, the magnitudes were found to differ from bearing to bearing. The comparison of the results indicates strong hardening features to be present at higher strain levels. Moreover, a strong dependence of the equilibrium hysteresis on the past maximum strain level was also appeared in the comparison. In addition, the equilibrium response was also found to be strongly dependent on the current strain values in all bearings.
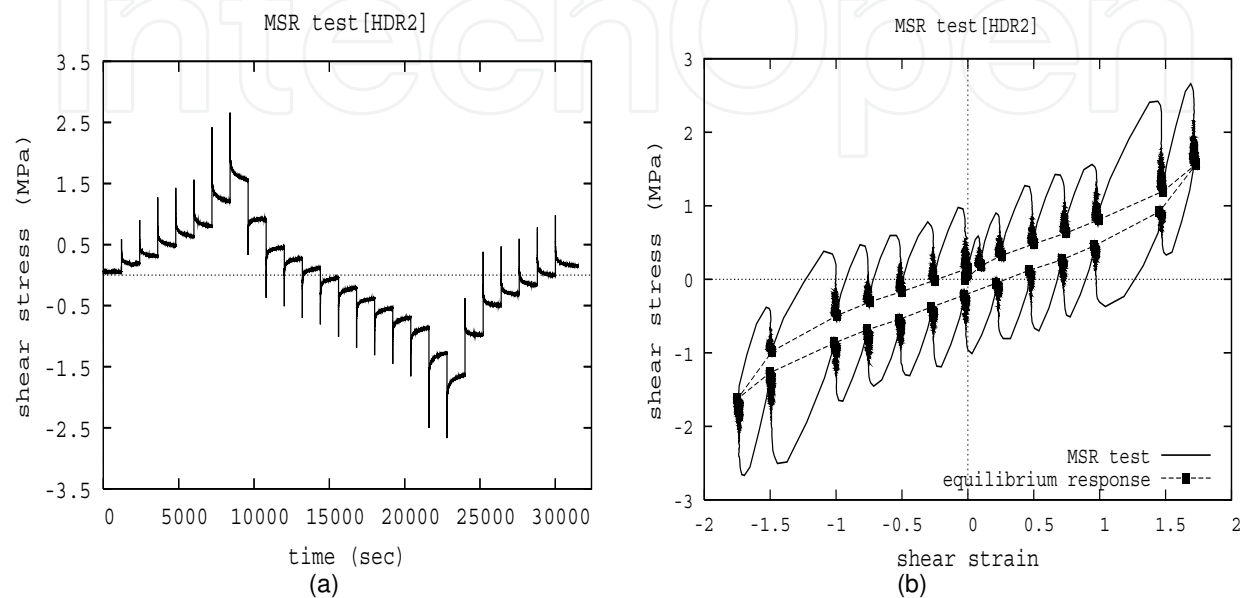

Figure 11. MSR test results of HDR2 (a) stress history (b) equilibrium stress response; equilibrium response at a particular strain level shows the response, which is asymptotically obtained from the shear stress histories of MSR test.

Figure 12. MSR test results of RB2 (a) stress history (b) equilibrium stress response; equilibrium response at a particular strain level shows the response, which is asymptotically obtained from the shear stress histories of MSR test.
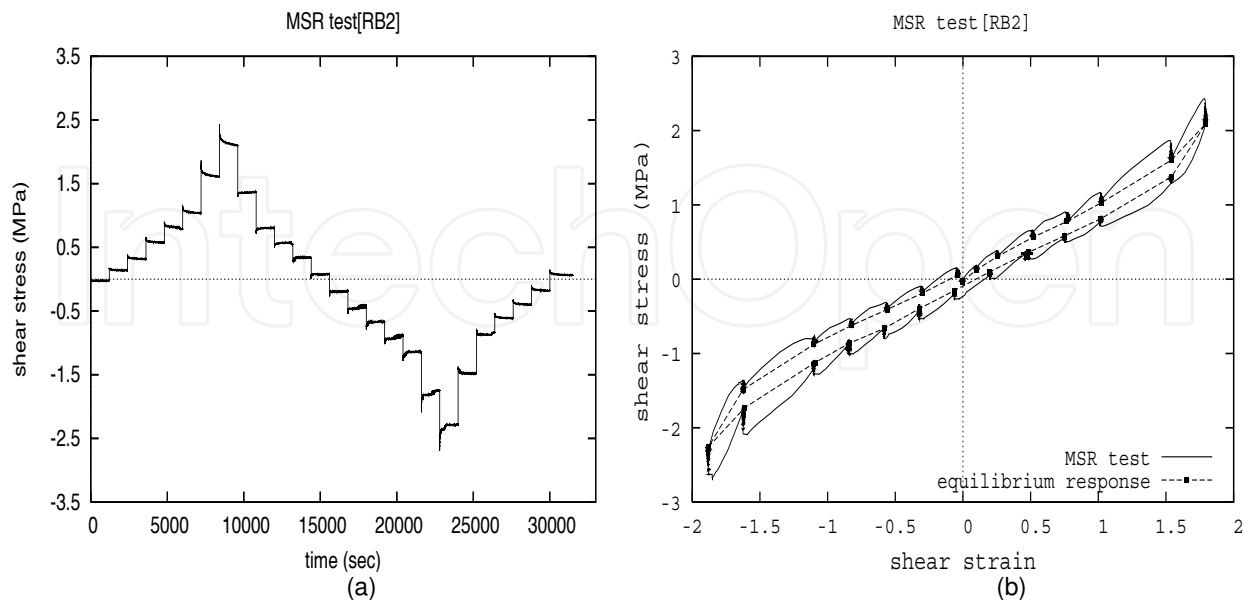
Figure 13. MSR test results of LRB2 (a) stress history (b) equilibrium stress response; equilibrium response at a particular strain level shows the response, which is asymptotically obtained from the shear stress histories of MSR tests.
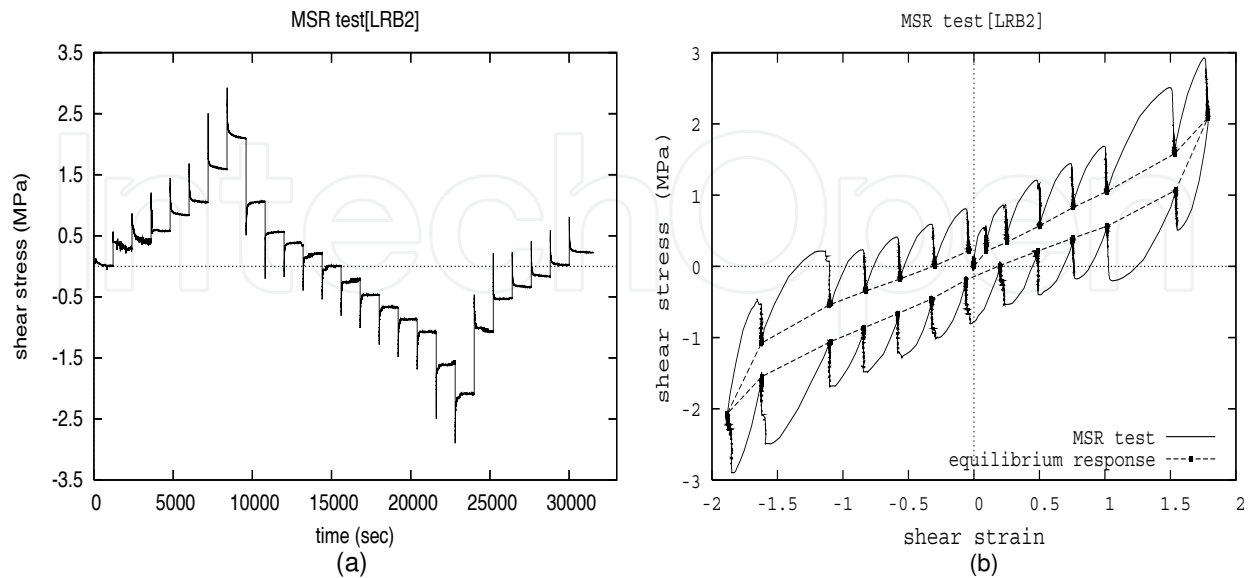

Figure 14. MSR test results of HDR2 at 2.50 maximum strain level (a) stress history (b) equilibrium stress response; equilibrium response at a particular strain level shows the response, which is asymptotically obtained from the shear stress histories of MSR test.

MSR test[RB2]

MSR test[RB2]

Figure 15. MSR test results of RB2 at 2.50 maximum strain level (a) stress history (b) equilibrium stress response; equilibrium response at a particular strain level shows the response, which is asymptotically obtained from the shear stress histories of MSR test.
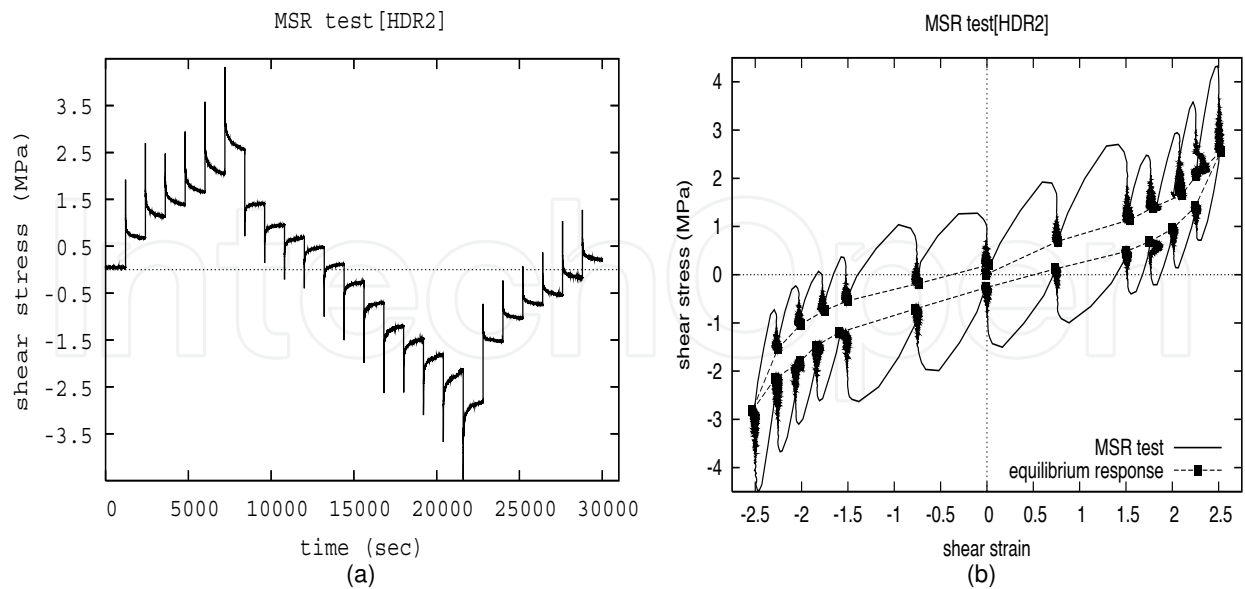
MSR test[LRB2]

MSR test[LRB2]

Figure 16. MSR test results of LRB2 at 2.50 maximum strain level (a) stress history (b) equilibrium stress response; equilibrium response at a particular strain level shows the response, which is asymptotically obtained from the shear stress histories of MSR test.
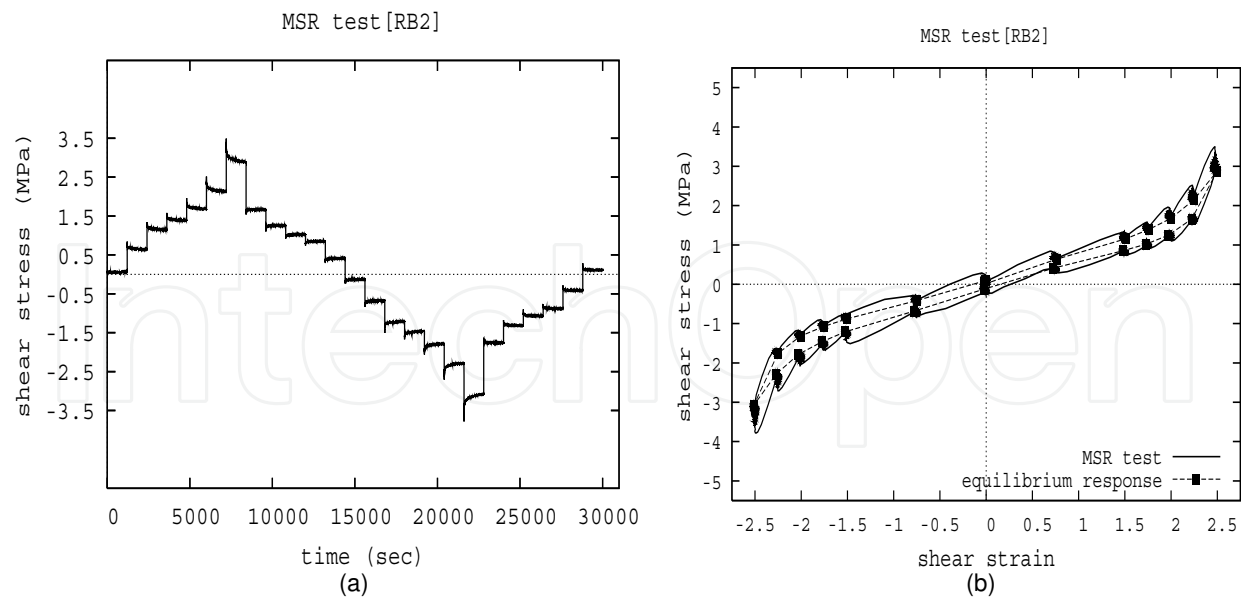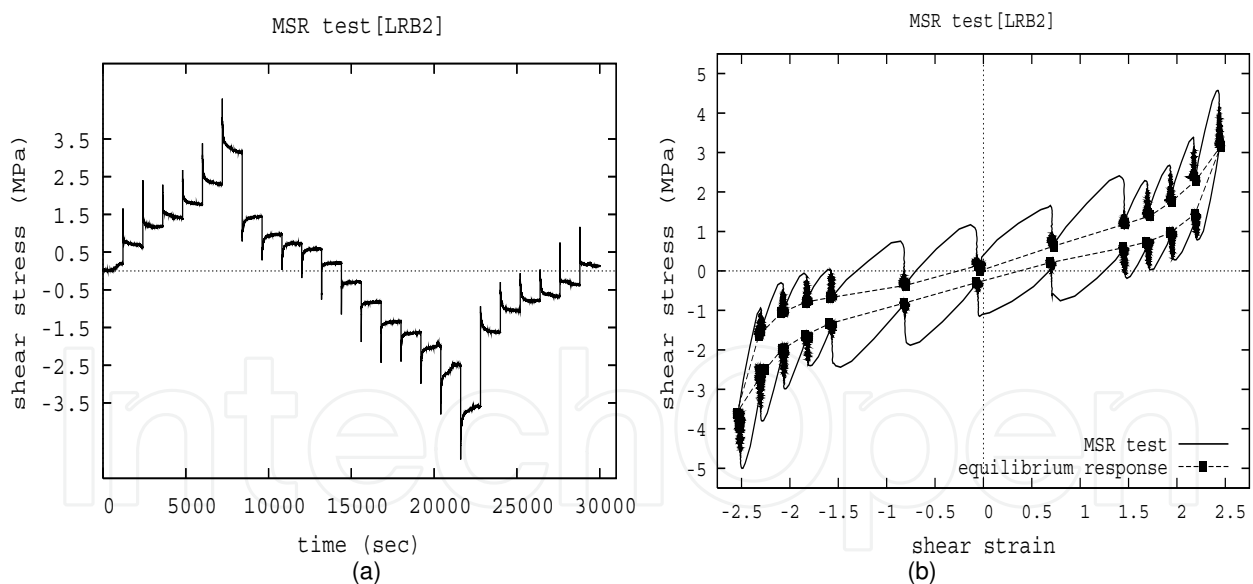
3. Structure of the rheology model

A rheology model for describing the three phenomenological effects of the bearings as mentioned above is constructed in this section. In Section 2, the Mullin's softening effect,

strain rate viscosity effect, strain dependent elasto-plastic behavior with hardening effect of the bearings are illustrated. As pointed out earlier that all the experiments were conducted on preloaded specimens and hence the Mullin's effect of the bearing was not considered in deriving the rheology model. The underlying key approach of constructing the model is an additive decomposition of the total stress response into three contributions associated with a nonlinear elastic ground-stress, an elasto-plastic stress, and finally a viscosity induced overstress. This approach has been motivated by the experimental observations (Section 2) of the bearings [33-35]. The decomposition can be visualized for one dimensional analogy of the rheology model as depicted in Figure 17 (a) and (b).The model is the extended version of the Maxwell's model by adding two branches: one branch is the nonlinear elastic spring element and the other one is the elastoplastic spring–slider elements.
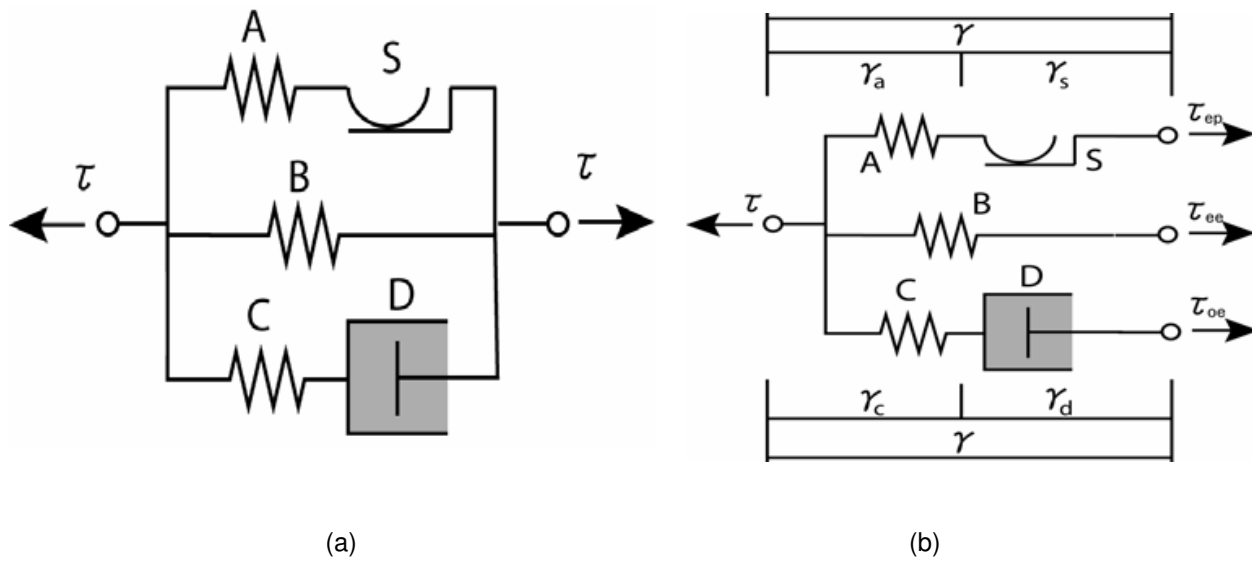

| (a) | (b) |

Figure 17. Structural configuration of the rheology model.

Motivated by the experimental observations, the mechanical behavior of the bearings can be also described as the sum of the two different behaviors: the rate-independent and the rate-dependent behaviors. The rate-independent behavior comprises the elasto-plastic and the nonlinear elastic response, which are represented in the top two branches of the model (Figures 17(a) and (b)). This phenomenon can be regarded as the equilibrium hysteresis to be identified from the relaxed equilibrium responses of the multi-step relaxations of the bearings. On the other hand, the rate-dependent response becomes very significant in relaxation and cyclic loading tests. The latter showed rate-dependent hysteresis loops where the size of the hysteresis increases with the increase of strain rates (Figures 7 (a) to (c)).

The total stress response of the bearing is motivated to decompose into three branches (Figure 17(b)):

$$\tau = \tau_{ep}(\gamma_a) + \tau_{ee}(\gamma) + \tau_{oe}(\gamma_c),$$ (3)

where τ_{ep} is the stress in the first branch composed of a spring (Element A) and a slider (Element S); τ_{ee} denotes the stress in the second branch with a spring (Element B); τ_{oe} represents the stress in the third branch comprising a spring (Element C) and a dashpot (Element D). The first and second branches represent the rate-independent elasto-plastic behavior, while the third branch introduces the rate-dependent viscosity behavior.

3.1. Modeling of equilibrium hysteresis

From the MSR test data (Figures 11 to 16), an equilibrium hysteresis loop with strain hardening is visible in each bearing. This equilibrium hysteresis loop can be suitably represented by combining the ideal elasto-plastic response (Figure 18a) and the nonlinear elastic response (Figure 18b).
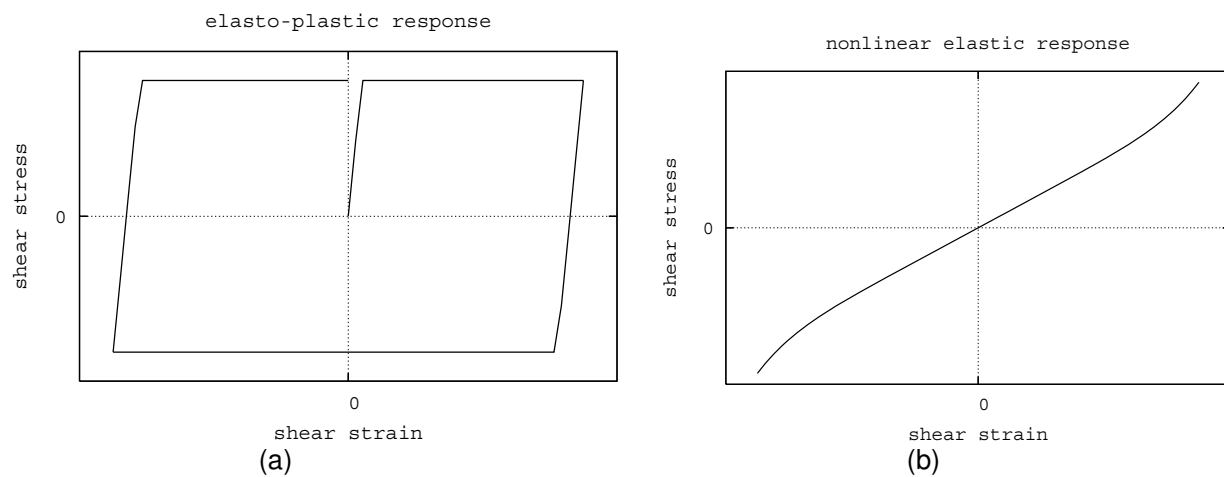

Figure 18. Formation of equilibrium hysteresis (a) elasto-plastic response (b) nonlinear elastic response.

The elasto-plastic response as shown in Figure 18(a) can be idealized by a spring-slider element as illustrated in Figure 19.
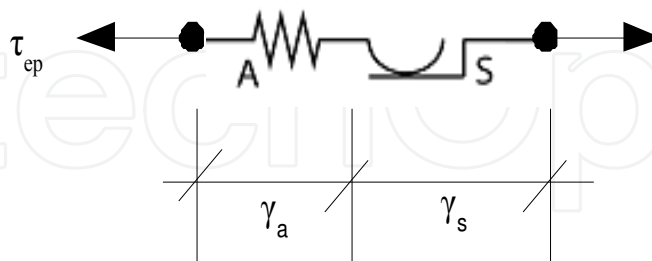

Figure 19. Spring-slider model for illustrating the rate-independent elasto-plasticity.

The total strain can be split into two components:

$$\gamma = \gamma_a + \gamma_s , \tag{4}$$

where γ_a stands for the strain on the spring (Element A), referred to as the *elastic part*, and γ_s is the strain on the slider(Element S), referred to as the *plastic part*.

From equilibrium consideration, the stress on the spring is τ_{ep}, and we have the elastic relationship

$$\tau_{ep} = C_1 \gamma_a ,$$ (5)

where C_1 is a spring constant for Element A.

The mechanical response of the slider (Element S) is characterized by the condition that the friction slider is active only when the stress level in the slider reaches a critical shear stress τ_{cr}, i.e., the stress τ_{ep} in the slider cannot be greater in absolute value than τ_{cr} which can be mathematically expressed as

$$\begin{cases} \dot{\gamma}_s \neq 0 & \text{for} \quad |\tau_{ep}| = \tau_{cr} \\ \dot{\gamma}_s = 0 & \text{for} \quad |\tau_{ep}| < \tau_{cr} \end{cases}$$ (6)

The evolution equation for the elastic strain γ_a can be written using the Eq.(5) as

$$\dot{\tau}_{ep} = \dot{\gamma} \left[U(\dot{\gamma}) U(\tau_{cr} - \tau_a) + U(-\dot{\gamma}) U(\tau_{cr} + \tau_a) \right]$$ (7)

with

$$U(x) = \begin{cases} 1 & : \quad x \geq 0 \\ 0 & : \quad x < 0 \end{cases}$$ (8)

The nonlinear elastic response as shown in Figure 18(b) with strain hardening at higher strain levels can be described by a non-Hookean nonlinear spring (Element B) (Figure 20):

$$\tau_{ee} = C_2 \gamma + C_3 |\gamma|^m \operatorname{sgn}(\gamma)$$ (9)

where C_2, C_3, and m $(m > 1)$ are constants with

$$\operatorname{sgn}(x) = \begin{cases} +1 & : \quad x > 0 \\ 0 & : \quad x = 0 \\ -1 & : \quad x < 0 \end{cases}$$ (10)
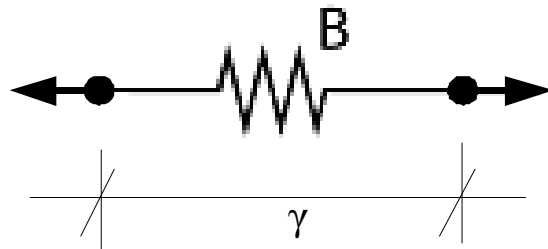

Figure 20. Non-Hookean spring element for illustrating the nonlinear elastic response.

Bearing /Pier	C_1	C_2	C_3	C_4	τ_{cr}	m
	MPa	MPa	MPa	MPa	MPa	
HDR1	2.401	0.535	0.002	2.805	0.205	8.182
HDR2	**2.502**	**0.653**	**0.006**	**3.254**	**0.247**	**6.621**
HDR3	2.101	0.595	0.002	2.653	0.296	7.423
LRB1	4.252	0.710	0.003	2.354	0.190	8.421
LRB2	**4.181**	**0.779**	**0.010**	**2.352**	**0.230**	**6.684**
RB1	1.953	0.798	0.005	0.401	0.130	7.853
RB2	**2.051**	**0.883**	**0.006**	**0.402**	**0.112**	**7.234**

Table 2. Rate-independent response parameters of the bearings
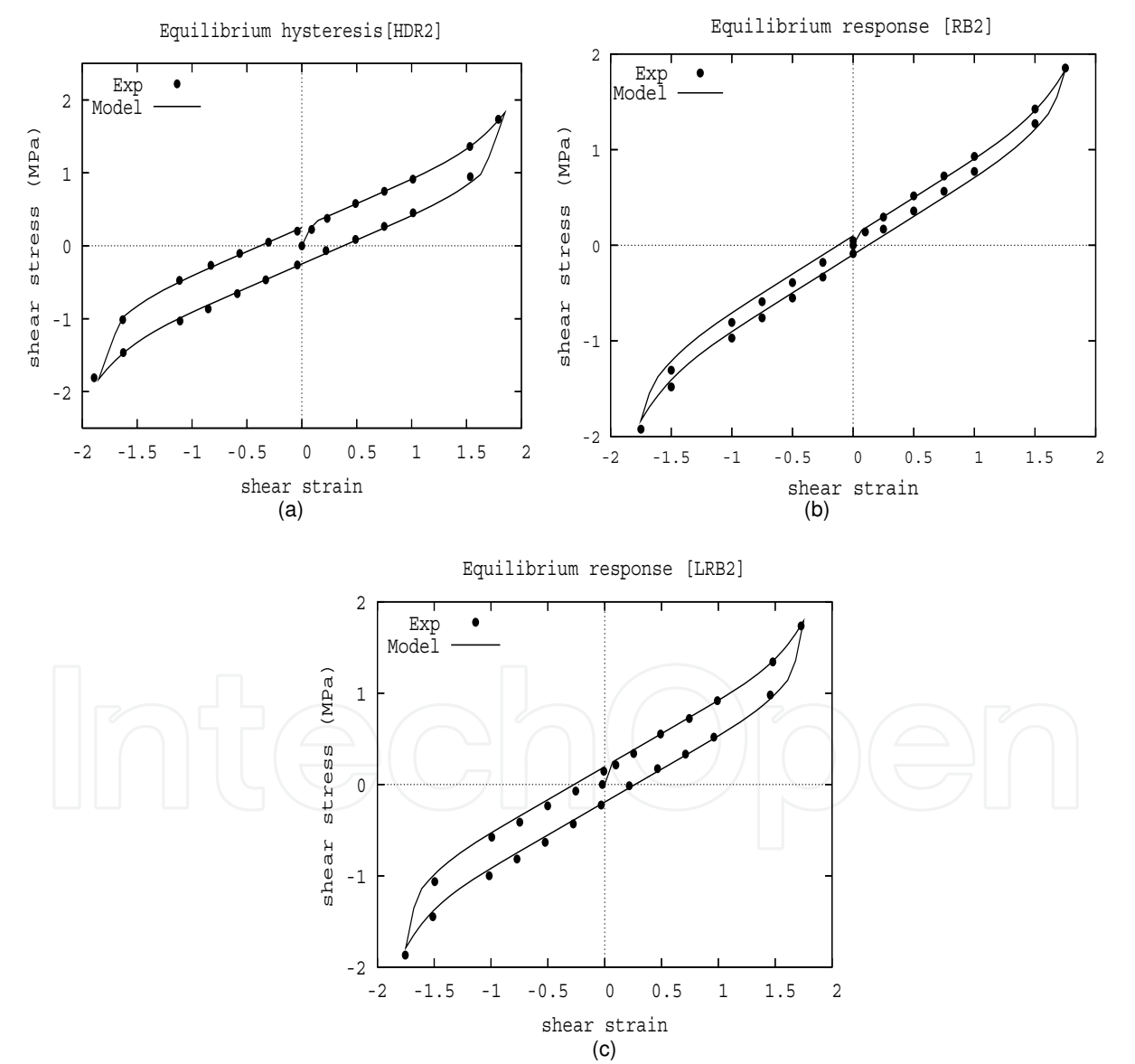

(a)

(b)

(c)

Figure 21. Identification of equilibrium response parameters for (a) HDR2, (b) RB2, and (c) LRB2; the experimental results are obtained from the MSR tests in asymptotic sense and the model results are determined using $\tau = \tau_{ee} + \tau_{ep}$ with parameters given in Table 2.

In order to determine the equilibrium response parameters as presented in Eqs. (5. 6 and 9), the equilibrium hysteresis loops as obtained from the MSR test have been considered. The equilibrium hysteresis loops of all bearings considered in the study are presented in Figures 21 (a) to (c). The experimental data are denoted by solid circular points. The critical shear, τ_{cr} is determined by using the equilibrium hysteresis loop. The difference between loading and unloading stresses in the equilibrium hysteresis loop at each strain level corresponds to $2\tau_{cr.}$ Accordingly, τ_{cr} can be determined from the half of the arithmetic average values of the stress differences. The parameter C_1 corresponding to the initial stiffness can then be determined by fitting the initial part as well as the switching parts from loading and unloading in the equilibrium hysteresis loop (see, for example, Figure 18(a)). Finally, the parameters for the nonlinear spring (Element B) are identified. The subtraction of the stress τ_{ep} of Eq.(5) from the equilibrium stress response obtained from the MSR test gives the stress τ_{ee} corresponding to Eq.(9).Parameters C_2, C_3, and m are determined using a standard least square method. The obtained critical stresses τ_{cr} and the equilibrium response parameters C_2, C_3, and m for all specimens are given in Table 2. The equilibrium responses obtained using the proposed model and the identified parameters are presented in Figures 21 (a) to (c). The solid line in each Figure shows the equilibrium responses obtained by the rheology model.

3.2. Modeling of instantaneous response

At the instantaneous state, the structure of the rheology model can be reduced into the same model without the dashpot element (Element D), because the dashpot is fixed ($\dot{\gamma}_d = 0$) owing to infinitely high strain-rate loading. Consequently, the instantaneous response of the rheology model can be obtained by adding τ_{oe} without Element D and the responses obtained from the other two branches as shown in Figure 22.
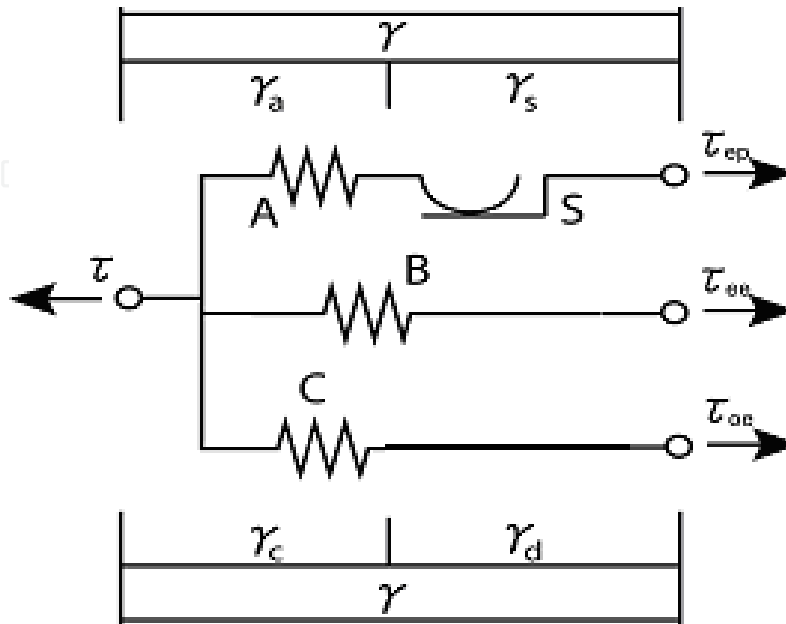

Figure 22. Spring-slider model for illustrating the instantaneous response.
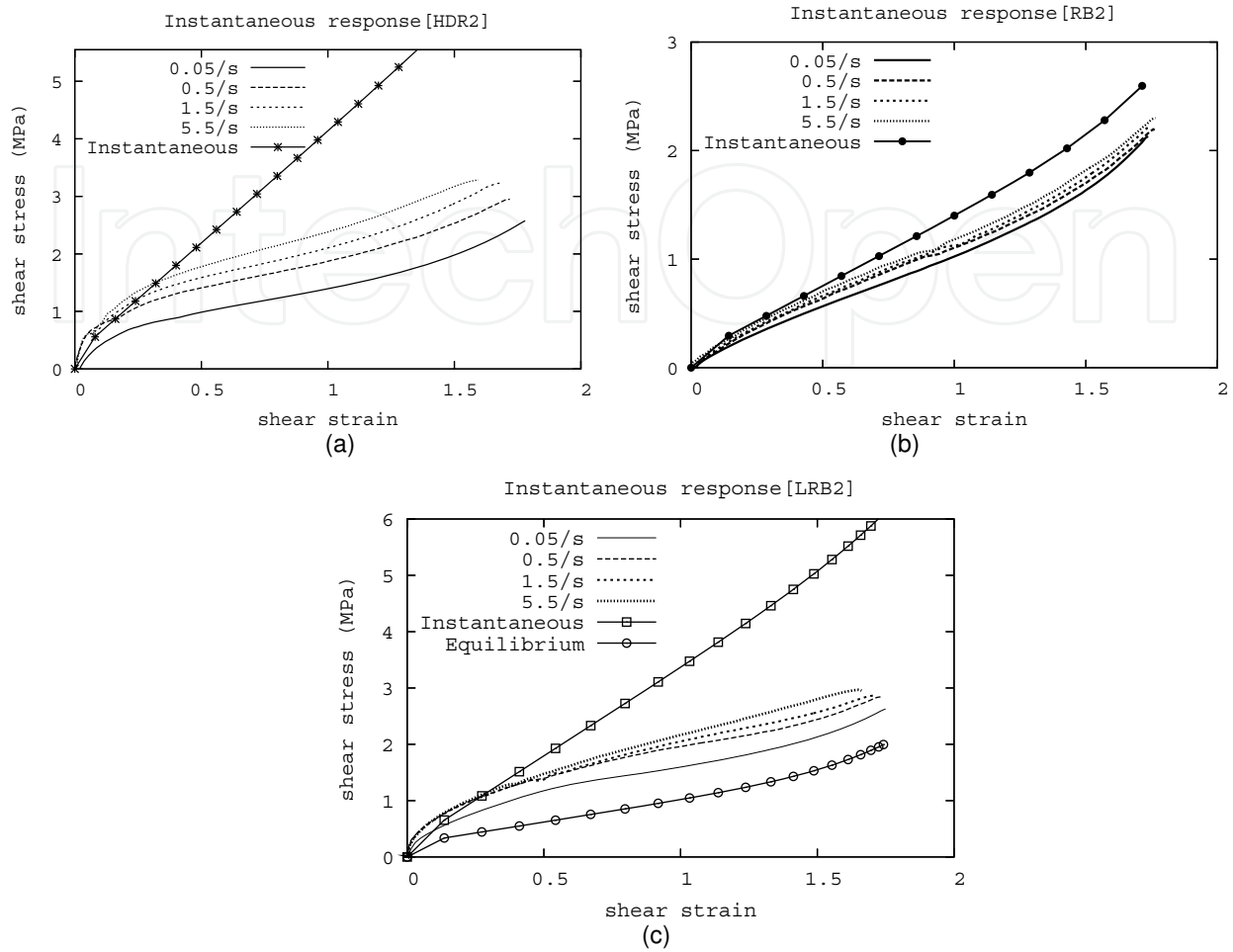
Figure 23. Identification of instantaneous response parameters for (a) HDR2, (b) RB2, and (c) LRB2; the instantaneous response is determined using the model $\tau = \tau_{ee} + \tau_{ep} + \tau_{oe}$(without dashpot element D) and the experimental results represented by different lines are obtained from CS tests at four strain rates of 0.05, 0.5, 1.5, and 5.5 /sec in loading regimes.

From the CS test results, a diminishing trend of the stress responses with increasing strain rates can be observed in all bearings as illustrated in Figures 7 (a) to (c). From these Figures, it has been observed that the instantaneous response lies at the neighborhood of the stress-strain curve at a strain rate of 5.5/s for the HDRB and the LRB; however for the RB, it is around the 1.5 /s strain rate. The instantaneous stress-strain curve, and accordingly the spring C seems to be nonlinear even in loading regime as clearly presented in Figures 23(a) to (c).

For simplicity, a linear spring model is employed for Element C in order to reproduce the instantaneous response of the bearings:

$$\tau_{oe} = C_4 \gamma_c , \tag{11}$$

where C_4 is the spring constant for Element C.

The parameter C_4 is determined so that the instantaneous stress-strain curve calculated from the rheology model ($\tau = \tau_{ee} + \tau_{ep} + \tau_{oe}$ (without the dashpot element)) can envelop the stress-strain curves obtained from the CS test. Figures 23(a) to (c) show comparison between the instantaneous stress-strain curves from the rheology model and those from the CS test at different strain rates up to 5.5/s in loading regime of all bearings. The obtained parameters C_4 for all bearings are listed in Table 2.

3.3. Modeling of nonlinear viscosity

Considering the third branch of the rheology model (Figure 17), the total strain can also be decomposed into two parts (Figure 24):

$$\gamma = \gamma_c + \gamma_d \tag{12}$$

where γ_c and γ_d stand for the strains in the spring (Element C) and the dashpot (Element D), respectively.
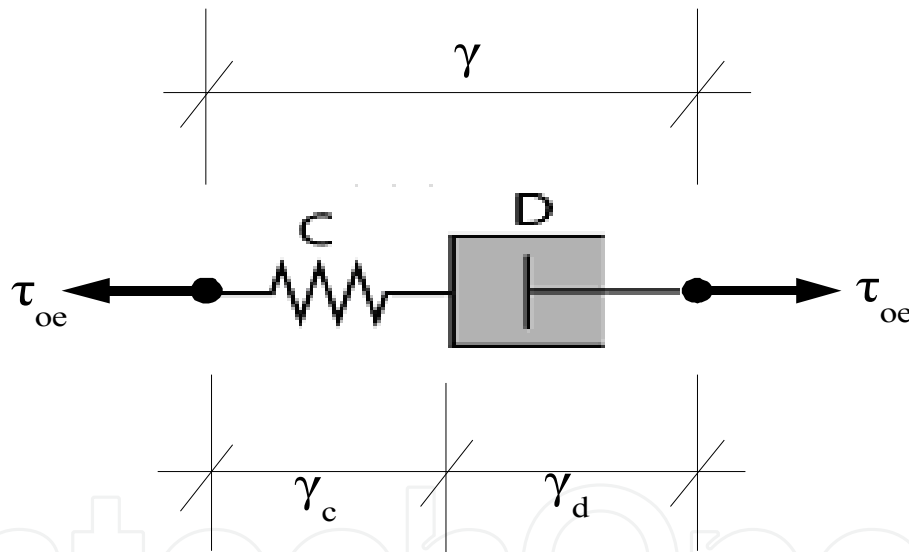

Figure 24. Spring-dashpot model for reproducing the rate-dependent stress response

The equilibrium condition of the stress components in the spring-dashpot elements states that the stress in the Element C must be equal to that in the Element D. The stress component in the Element C is expressed in Eq.(11). The evolution equation for the Element D has been constructed motivating by the experimental results of the bearings to be discussed in the following sub-sections. This section describes the procedure to identify the constitutive relationship of the dashpot (Element D) in the rheology model. To this end, the experimental results obtained from the MSR and the SR tests are analyzed to derive the relationship between the overstress τ_{oe} and the dashpot strain rate $\dot{\gamma}_d$. A schematic diagram to identify $\tau_{oe} - \dot{\gamma}_d$ relationship is presented in Figure 25.

From the stress relaxation results of the MSR and the SR loading tests, the time histories of the total stress τ and the total strain γ are obtained. Assuming that the asymptotic stress response at the end of each relaxation period is the equilibrium stress τ_{eq} at a particular strain level, the over stress history in each relaxation period is obtained by subtracting the equilibrium stress from the total stress. Then, the time history of the elastic strain for Element C is calculated from $\gamma_c = \tau_{oe}/C_4$ in Eq.(11), and consequently the time history of the dashpot strain can be determined as $\gamma_d = \gamma - \gamma_c$ using Eq. (12). In order to calculate the history of the dashpot strain rates, special treatment of the experimental data is required for taking the time derivatives over the experimental data points containing scattering due to noise. In order to reduce the scattering of experimental data, a moving averaging technique was employed in the current scheme before taking time derivatives of the experimental data points. All calculations were done by Mathematica [44].
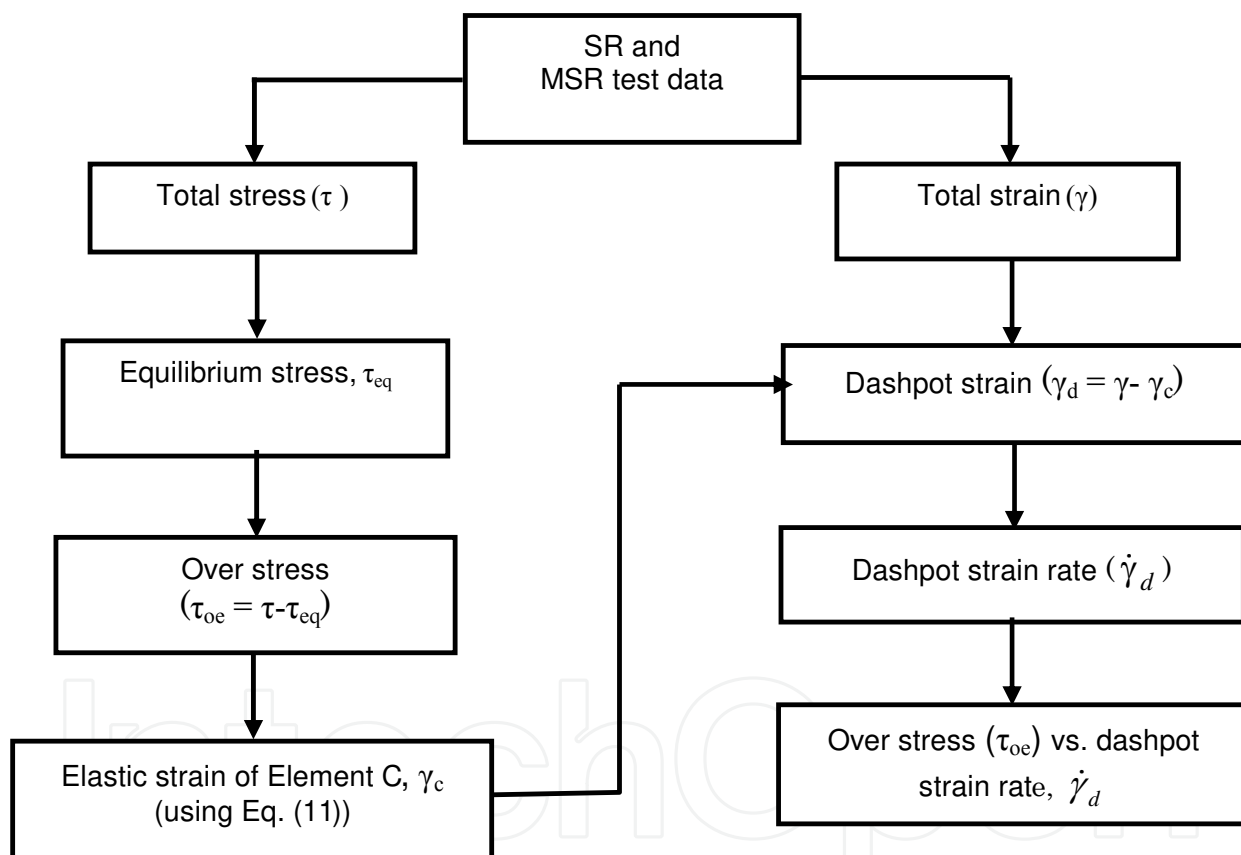
Figure 25. Schematic diagram to determine the analytical relationship between the over stress and the dashpot strain rates.

Figures 26(a) to (c) show the relationships between the overstress and the dashpot strain rates obtained from the MSR test results of the bearings (HDR2, RB2, and LRB2). In these Figures, the positive overstress indicates relaxation after loading, while the negative one does after unloading; (see Figure 10 for the strain histories of the MSR test). Figures 26 (a) to (c) demonstrate nonlinear dependence of the viscosity on the dashpot strain rates for all bearings. Since the gradient of $\tau_{oe} - \dot{\gamma}_d$ curves represents the viscosity, the viscosity

decreases with increasing dashpot strain rates. Furthermore, it is found that these relationships depend on the strain levels in the relaxation tests after loading; i.e. the overstress, and accordingly the viscosity increases with increasing the total strains. It should be noted that the dependence of the over stress on the total strain level after unloading is not significant as seen that after loading.

The same tendency of the stress responses have been apparently observed in SR tests which are illustrated in Figures 27(a) to (c). In SR tests, the total strains were assigned from 0 to 100, 150, 175% for loading, and then the strains were reduced to 0 for unloading (see Figure 8 for the strain histories). The values in the legend stand for the total strains in respective relaxation processes, and 100, 150, 175% correspond to relaxation process after loading, and 0% after unloading. While compared among the three bearings regarding the magnitude of the overstress at each strain level, HDR2 shows comparatively high overstress than the other two bearings, which are in agreement with the results of the CS tests (Figures 7 (a) to (c)).

In order to describe the nonlinear viscosity of the dashpot, it is necessary to distinguish loading and unloading with respect to the dashpot. The loading and unloading conditions are defined for the dashpot as follows:

$$\frac{\mathrm{d}}{\mathrm{dt}}\left|\gamma_d\right| > 0 \text{ for loading and } \frac{\mathrm{d}}{\mathrm{dt}}\left|\gamma_d\right| < 0 \text{ for unloading} \tag{13}$$

This loading-unloading condition is identical with

$$\tau_{oe}\gamma_d > 0 \text{ for loading and } \tau_{oe}\gamma_d < 0 \text{ for unloading} \tag{14}$$

Based on the $\tau_{oe} - \dot{\gamma}_d$ relationships obtained form the MSR and the SR test data shown in Figures 26 and 27 for the bearings, the constitutive model for the Element D can be expressed as

$$\begin{aligned}
\tau_{oe} &= A_l \exp\left(q|\gamma|\right)\mathrm{sgn}\left(\dot{\gamma}_d\right)\left|\frac{\dot{\gamma}_d}{\dot{\gamma}_o}\right|^n \text{ for loading,} \\
\tau_{oe} &= A_u \,\mathrm{sgn}\left(\dot{\gamma}_d\right)\left|\frac{\dot{\gamma}_d}{\dot{\gamma}_o}\right|^n \qquad \text{ for unloading,}
\end{aligned} \tag{15}$$

where $\dot{\gamma}_o = 1$ (sec^{-1}) is a reference strain rate of the dashpot; A_l, A_u, q and n are constants for nonlinear viscosity.

In SR and MSR tests, the loading/unloading condition changes abruptly (e.g. Figures 8 to 10). However, under general loading histories, the loading/unloading condition may change gradually. To avoid abrupt change in viscosity due to a shift in the loading and unloading conditions, a smooth function is introduced into the overstress expression, which facilitates the Eq.(15a,b) to be rewritten in a more compact form

$$\tau_{oe} = A \left| \frac{\dot{\gamma}_d}{\dot{\gamma}_o} \right|^n \text{sgn}(\dot{\gamma}_d)$$

with

(16)

$$A = \frac{1}{2}\left(A_l \exp(q|\gamma|) + A_u\right) + \frac{1}{2}\left(A_l \exp(q|\gamma|) - A_u\right)\tanh(\xi\tau_{oe}\gamma_d)$$

where ξ is the smoothing parameter to switch viscosity between loading and unloading. Now, in the subsequent paragraphs, the procedure for determining the viscosity constants (A_l, A_u, q and n) will be discussed followed by the smoothing parameter (ξ).

Bearing /Pier	A_l MPa	A_u MPa	q	n	ξ
HDR1	0.501	0.904	0.532	0.205	1.221
HDR2	**0.982**	**0.952**	**0.344**	**0.224**	**1.252**
HDR3	0.754	0.753	0.353	0.213	1.242
LRB1	0.731	0.731	0.0	0.272	0.0
LRB2	**0.792**	**0.792**	**0.0**	**0.302**	**0.0**
RB1	0.552	0.552	0.0	0.232	0.0
RB2	**0.434**	**0.434**	**0.0**	**0.243**	**0.0**

Table 3. Rate-dependent viscosity parameters of the HDRB

Using the strain histories of the SR loading tests at different strain levels (Figure 8), the overstress-dashpot strain rates relationships are determined (Figures 27 (a) to (c)), which correspond to Eq.16 for both loading and unloading conditions. A standard method of nonlinear regression analysis is employed in Eq. 16 to identify the viscosity constants. As motivated by the relationships of the overstress-dashpot strain rates obtained in the SR/MSR test results, the value of n is kept the same in loading and unloading conditions. The nonlinear viscosity parameters obtained in this way are presented in Table 3. Figures 27(a) to (c) present the overstress-dashpot strain rates relationships obtained using the proposed model and the SR test results; the solid lines show the model results and the points do for the experimental data.

A sinusoidal loading history is utilized to determine the smoothing parameter of the model (Eq.16). The sinusoidal loading history corresponds to a horizontal shear displacement history applied at the top of the bearing at a frequency of 0.5 Hz with amplitude of 1.75. An optimization method based on Gauss-Newton algorithm [45] is employed to determine the smoothing parameter. The optimization problem is mathematically defined as minimizing the error function presented as

$$\text{Minimize}\left\{ E(\xi, t) = \sum_{n=1}^{N}\left(\tau_{exp,n} - \tau_{m,n}\right)^2 \right\},$$

(17)

where N represents the number of data points of interest, $\tau_{exp,n}$ and $\tau_{m,n}$ imply the shear stress responses at time t_n obtained from the experiment and the model, respectively, and ξ stands for the parameter to be identified. Using the Gauss-Newton algorithm, following condition is satisfied for obtaining the minimum error function as

$$\nabla E\left(\xi_i,t\right) + \nabla^2 E\left(\xi_i,t\right)\left(\xi_{i+1}-\xi_i\right) = 0 , \tag{18}$$

where ∇ refers the gradient operator. During the iteration process, the updated parameter in each iteration is determined using

$$\xi_{i+1} = \xi_i - \delta\frac{\nabla E\left(\xi_i,t\right)}{\nabla^2 E\left(\xi_i,t\right)} , \tag{19}$$

where δ is the numerical coefficient between 0 and 1 to satisfy the Wolfe conditions at each step of the iteration. The values of ξ determined in this way for the bearings are presented in Table 3.
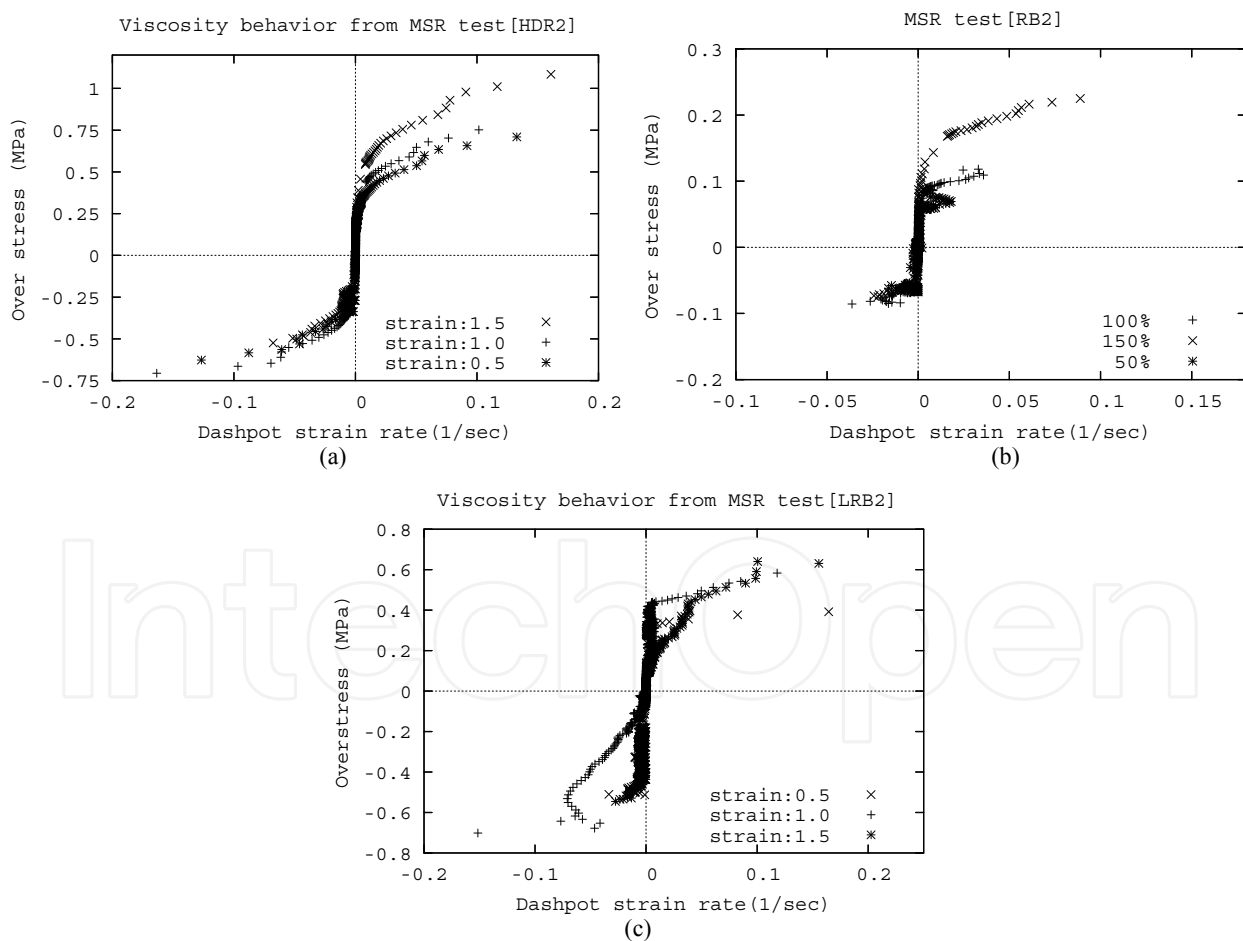

Figure 26. Overstress-dashpot strain rate relation obtained from the MSR tests at different strain levels in loading and unloading regimes of (a) HDR2, (b) RB2, and (c) LRB2; the values in the legend stand for the total strain in respective relaxation processes, and 50,100, 150% correspond to relaxation processes after loading and unloading.
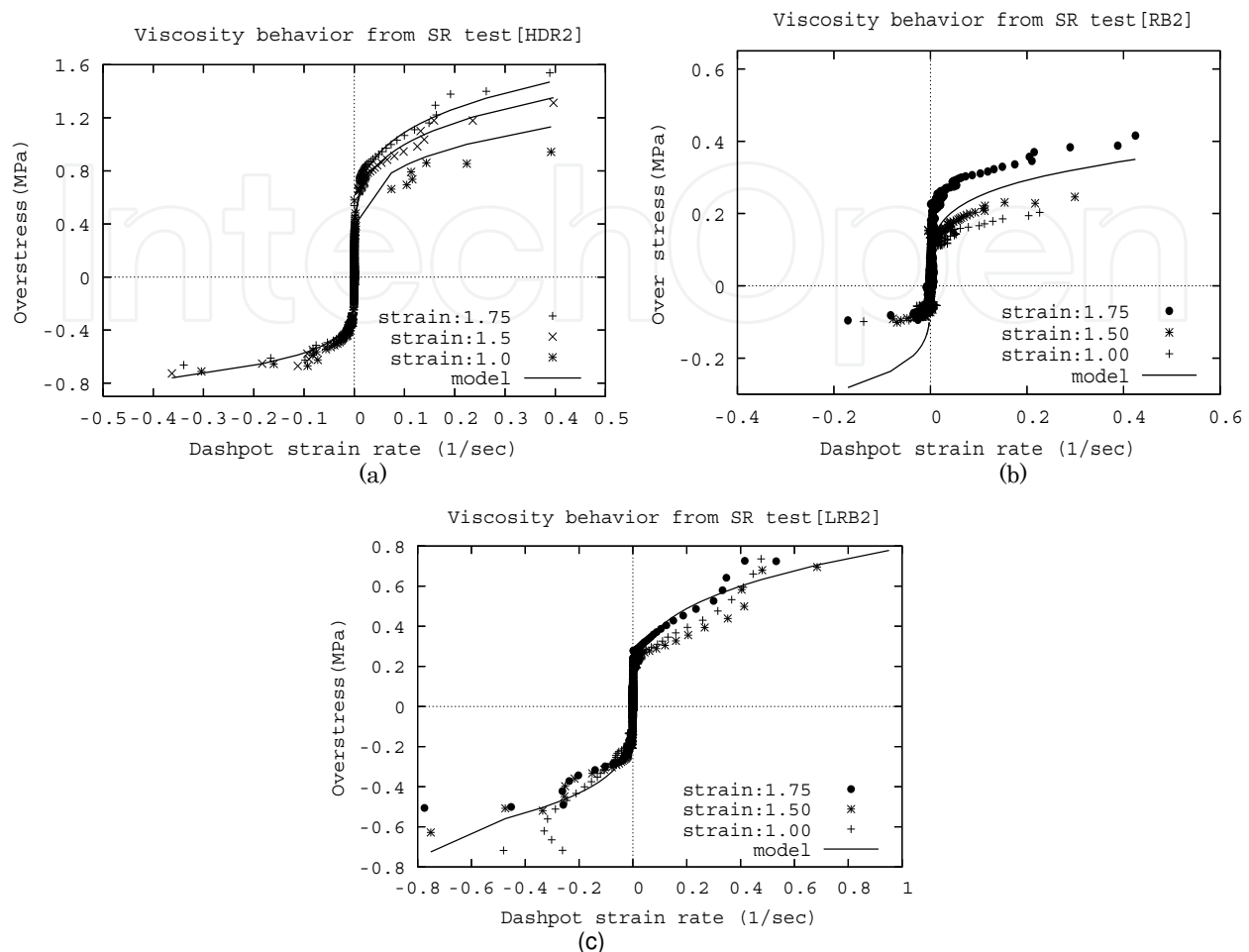
Figure 27. Identification of viscosity parameters of (a) HDR2, (b) RB2, and (c) LRB2; the model results represented by solid lines are obtained by $\tau = \tau_{oe}$ with parameters given in Table 3 and the relations between $\tau_{oe} - \dot{\gamma}_d$ as calculated from SR test data are shown by points. The values in the legend stand for the total strain in respective relaxation processes, and 100,150, 175% correspond to relaxation processes after loading, and 0% after unloading.

4. Thermodynamic consistency of the rheology model

The Clausisus-Duhem inequality is a way of expressing the second law of thermodynamics used in continuum mechanics. This inequality is particularly useful in determining whether the given constitutive relations of material/solid are thermodynamically compatible [46]. This inequality is a statement concerning the irreversibility of natural resources, especially when energy dissipation is involved. The compatibility with the Clausisus-Duhem inequality is also known as the thermodynamic consistency of solid. This consistency implies that constitutive relations of solids are formulated so that the rate of the specific entropy production is non-negative for arbitrary temperature and deformation processes.

In this context, the Clausius-Duhem inequality reads

$$-\rho\dot{\psi} + \tau\dot{\gamma} \geq 0 \,, \tag{21}$$

where ρ is the mass density, ψ is the Helmholtz free energy per unit mass, and $\tau\dot{\gamma}$ is the stress power per unit volume. It states that the supplied stress power has to be equal or greater than the time rate of the Helmholtz free energy. For the rheology model, the Helmholtz free energy is the mechanical energy stored in the three springs shown in Figure 17 can be represented as

$$\rho\psi(\gamma,\gamma_a,\gamma_c) = \frac{1}{2}C_1\gamma_a^2 + \frac{1}{2}C_2\gamma^2 + \frac{C_3}{m+1}|\gamma|^{m+1} + \frac{1}{2}C_4\gamma_c^2 \tag{22}$$

Its time-rate reads as follows

$$\rho\dot{\psi}(\gamma,\gamma_a,\gamma_c) = C_1\gamma_a\dot{\gamma}_a + C_2\gamma\dot{\gamma} + C_3|\gamma|^m\dot{\gamma} + C_4\gamma_c\dot{\gamma}_c \tag{23}$$

The stress power of the model is

$$\tau\dot{\gamma} = (\tau_{ee} + \tau_{ep} + \tau_{oe})\dot{\gamma} = \tau_{ee}\dot{\gamma} + \tau_{ep}(\dot{\gamma}_a + \dot{\gamma}_s) + \tau_{oe}(\dot{\gamma}_c + \dot{\gamma}_d) \tag{24}$$

Inserting the stress power (Eq.24) and the time-rate of the Helmholtz free energy (Eq.23) into the 2nd law of thermodynamics (Eq. 21) and rearranging the terms leads to the following expression (Eq.25)

$$(\tau_{ep} - C_1\gamma_a)\dot{\gamma}_a + (\tau_{ee} - C_2\gamma - C_3|\gamma|^m)\dot{\gamma} + (\tau_{oe} - C_4\gamma_c)\dot{\gamma}_c + \tau_{ep}\dot{\gamma}_s + \tau_{oe}\dot{\gamma}_d \geq 0 \tag{25}$$

In order to satisfy this inequality for arbitrary values of the strain-rates of the variables in the free energy, the following equations for the three stress components which correspond to Eqs.(5), (9) ,and (11), respectively, yield

$$\tau_{ep} = C_1\gamma_a \,,\ \tau_{ee} = C_2\gamma + C_3|\gamma|^m \operatorname{sgn}(\gamma) \,,\ \text{and}\ \tau_{oe} = C_4\gamma_c \tag{26}$$

The residual inequality to be satisfied is

$$\tau_{ep}\dot{\gamma}_s + \tau_{oe}\dot{\gamma}_d \geq 0 \tag{27}$$

It states that the inelastic stress-powers belonging to the two dissipative elements (Element S and Element D) have to be non-negative for arbitrary deformation processes. Assuming that the time-derivatives of the inelastic deformations are the same sign as the corresponding stress quantities, each of the product terms of Eq. (27) is ensured to be non-negative with parameters given in Table 3. The non-negative dissipation energy of the bearings is ensured only when all the parameters responsible for expressing the elasto-plastic stress (τ_{ep}) and

the viscosity induced overstress (τ_{oe}) are non-negative. The parameters of Table 3 have confirmed this condition.

5. Summary

This chapter discusses an experimental scheme to characterize the mechanical behavior of three types of bearings and subsequently demonstrates the modeling approaches of the stress responses identified from the experiments. The mechanical tests conducted under horizontal shear displacement along with a constant vertical compressive load demonstrated the existence of Mullins' softening effect in all the bearing specimens. However, with the passage of time a recovery of the softening effect was observed. A preloading sequence had been applied before actual tests were carried out to remove the Mullins' effect from other inelastic phenomena. Cyclic shear tests carried out at different strain rates gave an image of the significant strain-rate dependent hysteresis property. The strain-rate dependent property in the loading paths was appeared to be reasonably stronger than in the unloading paths. The simple and multi-step relaxation tests at different strain levels were carried out to investigate the viscosity property in the loading and unloading paths of the bearings. Moreover, in order to identify the equilibrium hysteresis, the multi-step relaxation tests were carried out with different maximum strain levels. The dependence of the equilibrium hysteresis on the experienced maximum strain and the current strain levels was clearly demonstrated in the test results.

The mechanical tests indicated the presence of strain-rate dependent hysteresis with high strain hardening features at high strain levels in the HDRB. In the other bearing specimens, strain-rate dependent phenomenon was seen less prominent; however, the strain hardening features at high strain levels in the RB showed more significant than any other bearings. In this context, an elasto-plastic model was proposed for describing strain hardening features along with equilibrium hysteresis of the RB, LRB and HDRB. The performance of the proposed model in representing the strain rate-independent responses of the bearings was evaluated. In order to model the strain-rate dependent hysteresis observed in the experiments, an evolution equation based on viscosity induced overstress was proposed for the bearings. In doing so, the Maxwell's dashpot-spring model was employed in which a nonlinear viscosity law is incorporated. The nonlinear viscosity law of the bearings was deduced from the experimental results of MSR and SR loading tests. The performance of the proposed evolution equation in representing the rate-dependent responses of the bearings was evaluated using the relaxation loading tests. On the basis of the physical interpretation of the strain-rate dependent hysteresis along with other inelastic properties observed in the bearings, a chronological method comprising of experimentation and computation was proposed to identify the constitutive parameters of the model. The strain-rate independent equilibrium response of the bearing was identified using the multi-step relaxation tests. After identifying this response, the elasto-plastic model (the top two branches of the rheology model) was used to find out the parameters for the elasto-plastic response. A series

of cyclic shear tests were utilized to estimate the strain-rate independent instantaneous response of the bearings. A linear elastic spring element along with the elasto-plastic rheology model (the rheology model without the dashpot element) was used to determine the parameters of the instantaneous responses. After determining the elasto-plastic parameters of the bearings, the proposed evolution equation based on the viscosity induced overstress was used to find out the viscosity parameters by comparing the simple relaxation test data. Moreover, a mathematical equation involving smoothing function was proposed to establish loading and unloading conditions of the overstress; and sinusoidal loading data was then used to estimate the smoothing parameter of the overstress. Finally, the thermodynamic compatibility was confirmed by expressing the rheology model by using the Clausius-Duhem inequality equation.

Author details

A. R. Bhuiyan
Department of Civil Engineering, Chittagong University of Engineering and Technology, Chittagong, Bangladesh

Y.Okui
Department of Civil and Environmental Engineering, Saitama University, Saitama, Japan

Acknowledgement

6. References

[1] Skinner R I, Robinson W H, and McVerry G H. An Introduction to Seismic Isolation. DSIR Physical Science, Wellington, New Zealand; 1993.

[2] Kelly J M. Earthquake Resistant Design with Rubber. 2nd edition, Springer-Verlag Berlin Heidelberg, New York;1997.

[3] Naeim F and Kelly J. Design of Seismic Isolated Structures. 1st edition, John Wiley and Sons, New York; 1996.

[4] Priestley M J N, Seible F and Calvi G M. Seismic Design and Retrofit of Bridges. John Wiley and Sons, New York; 1996.

[5] Kelly J M Buckle I G. and Tsai H C. Earthquake Simulator Testing of a Base-Isolated Bridge Deck. UCB/EERC/ 85-09; 1985.

[6] Igarashi A and Iemura H. Experimental and Analytical Evaluation of Seismic Performance of Highway Bridges with Base Isolation Bearings. Proceedings of the 9th World Conference on Earthquake Engineering, Tokyo, Japan, Paper No. 553; 1996.

[7] Mori A, Carr A J, Cooke N and Moss P J. Compression Behavior of Bridge Bearings used for Seismic Isolation. Engineering Structures 1996; 18 351-362.

[8] Mori A, Moss P J, Cooke N, and Carr A J. The Behavior of Bearings used for Seismic Isolation under Shear and Axial Load. Earthquake Spectra 1999; 15 199-224.

[9] Burstscher S, Dorfmann A, and Bergmeister K. Mechanical Aspects of High Damping Rubber. Proceedings of the 2nd International PhD Symposium in Civil Engineering, Budapest, Hungary; 1998.

[10] Fujita T, Suzuki S and Fujita S. Hysteretic Restoring Force Characteristics of High Damping Rubber Bearings for Seismic Isolation. Proceedings of ASME PVP Conference, PVP, 181, 35-41; 1989.

[11] Mazda T, Shiojiri H, Oka Y, Fujita T and Seki M. Test on Large-Scale Seismic Isolation Elements. Transactions of the 10th International Conference on SMiRT-K, 678-685; 1989.

[12] Ohtori Y, Ishida K and Mazda T. Dynamic Characteristics of Lead Rubber Bearings with Dynamic Two Dimensional Test Equipment. ASME Seismic Engineering, PVP Conference, 2,145-153; 1994.

[13] Robinson W H. Lead Rubber Hysteresis Bearings Suitable for Protecting Structures during Earthquakes. Earthquake Engineering and Structural Dynamics 1982; 10 593-604.

[14] Abe M, Yoshida J and Fujino Y. Multiaxial Behaviors of Laminated Rubber Bearings and their Modeling. I: Experimental Study. Journal of Structural Engineering 2004; 130 1119-1132.

[15] Aiken I D, Kelly J M and Clark P W. Experimental Studies of The Mechanical Characteristics of Three Types of Seismic Isolation Bearings. Proceedings of the 10th World Conference of Earthquake Engineering (WCEE), Madrid, Spain, 2280-2286; 1992.

[16] Kikuchi M and Aiken I D. An Analytical Hysteresis Model for Elastomeric Seismic Isolation Bearings. Earthquake Engineering and Structural Dynamics 1997; 26 215-231.

[17] Sano T, Di and Pasquale G. A Constitutive Model for High Damping Rubber Bearings. Journal of Pressure Vessel Technology 1995; 117 53-57.

[18] Dall'Asta A and Ragni L. 2006. Experimental Tests and Analytical Model of High Damping Rubber Dissipating Devices. Engineering Structures 1995; 28 1874-1884.

[19] Hwang J S, Wu J D, Pan T C, and Yang G. A Mathematical Hysteretic Model for Elastomeric Isolation Bearings. Earthquake Engineering and Structural Dynamics 2002; 31 771-789.

[20] Tsai C S, Chiang Tsu-Cheng Chen Bo-Jen band Lin Shih-Bin. An Advanced Analytical Model for High Damping Rubber Bearings. Earthquake Engineering and Structural Dynamics 2003; 32 1373-1387.

[21] Amin A F M S, Alam M S and Okui Y. An Improved Hyperelasticity Relation in Modeling Viscoelasticity Response of Natural and High Damping Rubbers in Compression: Experiments, Parameter Identification and Numerical Verification. Mechanics of Materials 2002; 34 75-95.

[22] Amin A F M S, Wiraguna S I, Bhuiyan, A R and Okui Y. Hyperelasticity Model for Finite Element Analysis of Natural and High Damping Rubbers in Compression and Shear. Journal of Engineering Mechanics 2006; 132 54-64.

[23] Bergstrom J S and Boyce M C. Constitutive Modeling of the Large Strain Time-Dependent Behavior of Elastomers. Journal of the Mechanics and Physics of Solids 1998; 46 931-954.

[24] Haupt P and Sedlan K. Viscoplasticity of Elastomeric Materials: Experimental Facts and Constitutive Modeling, Archive of Applied Mechanics 2001; 71 89-109.

[25] Lion A. A Constitutive Model for Carbon Black Filled Rubber: Experimental Investigations and Mathematical Representation. Continuum Mechanics and Thermodynamics 1996; 8 153-169.

[26] Miehe C and Keck J. Superimposed Finite Elastic-Viscoplastic-Plasto-Elastic Stress Response with Damage in Filled Rubbery Polymers. Experiments, Modeling and Algorithmic Implementation. Journal of Mechanics and Physics of Solids 2000; 48 323-365.

[27] Spathis G. and Kontou E. Modeling of Nonlinear Viscoelasticity at Large Deformations. Journal of Material Science 2008; 43 2046-2052.

[28] Amin A F M S, Lion A, Sekita S and Okui Y. Nonlinear Dependence of Viscosity in Modeling the Rate-Dependent Response of Natural and High Damping Rubbers in Compression and Shear: Experimental Identification and Numerical Verification. International Journal of Plasticity 2006; 22 1610-1657.

[29] Bergstrom J S and Boyce M C. Large Strain Time-Dependent Behavior of Filled Elastomers. Mechanics of Materials 2000; 32 627-644.

[30] Mullins L. Softening of Rubber by Deformation. Rubber Chemistry and Technology 1969; 42 339-362.

[31] Gent A N. Relaxation Processes in Vulcanized Rubber I: Relation among Stress Relaxation, Creep, Recovery and Hysteresis. Journal of Applied Polymer Science 1962; 6 433-441.

[32] International Organization of Standardization (ISO). Elastomeric Seismic-Protection Isolators, Part 1: Test methods, Geneva, Switzerland; 2005.

[33] Bhuiyan A R. Rheology Modeling of Laminated Rubber Bearings for Seismic Analysis. PhD thesis. Saitama University, Saitama, Japan; 2009

[34] Bhuiyan A R, Okui Y, Mitamura H and Imai T. A Rheology Model of High Damping Rubber Bearings for Seismic Analysis: Identification of Nonlinear Viscosity. International Journal of Solids and Structures 2009; 46 1778-1792.

[35] Imai T , Bhuiyan A R, Razzaq M K, Okui Y and Mitamura H. Experimental Studies of Rate-Dependent Mechanical Behavior of Laminated Rubber Bearings. Joint Conference Proceedings of 7th International Conference on Urban Earthquake Engineering (7CUEE) & 5th International Conference on Earthquake Engineering (5ICEE), March 3-5, 2010, Tokyo Institute of Technology, Tokyo, Japan; 2010.

[36] Bueche F. Moelcular Basis for the Mullins Effect. Journal of Applied Polymer Science 1960; 4 107-114.

[37] Bueche F. Mullins Effect and Rubber-Filler Interaction. Journal of Applied Polymer Science 1961; 5 271-281.

[38] Burtscher S and Dorfmann A. Compression and Shear Tests of Anisotropic High Damping Rubber Bearings. Engineering Structures 2004; 26 1979-1991.

[39] Treloar L R G. The Physics of Rubber Elasticity. 3rd edition, Oxford University Press; 1975.

[40] Besdo D and Ihlemann J. Properties of Rubber Like Materials under Large Deformations Explained By Self-Organizing Linkage Patterns. International Journal of Plasticity 2003; 19 1001-1018.

[41] Ihlemann J. Modeling of Inelastic Rubber Behavior under Large Deformations Based on Self-Organizing Linkage Patterns. Constitutive Models for Rubber, Balkema, Rotterdam; 1999.

[42] Lion A. A Physically Based Method to Represent the Thermo-Mechanical Behavior of Elastomers. Acta Mechanica 1997; 123 1-25.

[43] Kilian H G, Strauss M and Hamm W. Universal Properties in Filler-Loaded Rubbers. Rubber Chemistry and Technology 1994; 67 1-16.

[44] Wolfram Research Inc. Mathematica Version 5.2, USA; 2005.

[45] Venkataraman P. Applied Optimization with Matlab Programming. John Wiley and Sons, New York; 2002.

[46] Truesdell C. The Mechanical Foundations of Elasticity and Fluid Dynamics. Journal of Rational Mechanics and Analysis 1952; 1 125–300.